Bioluminescence Imaging Strategies for Tissue Engineering Applications

Sarah Julia Lapp

Thesis submitted to the Faculty of the
Virginia Polytechnic Institute and State University
in partial fulfillment of the requirements for the degree of

Master of Science
In
Biomedical Engineering

Committee Members:

Aaron S. Goldstein, chair
Abby W. Morgan
Ge Wang

April 26, 2010
Blacksburg, VA

Keywords: bone tissue engineering, bioluminescence imaging, bone morphogenetic protein-2, flow perfusion

Bioluminescence Imaging Strategies for Tissue Engineering Applications

Sarah Julia Lapp

Abstract

In vitro differentiation of stem cells in biocompatible scaffolds in a bioreactor is a promising method for creating functional engineered tissue replacements suitable for implantation. Basic studies have shown that mechanical, chemical, and pharmaceutical stimuli enhance biological functionality of the replacement as often defined by parameters such as cell viability, gene expression, and protein accumulation. Most of the assays to evaluate these parameters require damage or destruction of the cell-scaffold construct. Therefore, these methods are not suitable for monitoring the development of a functional tissue replacement in a spatial and temporal manner prior to implantation. Bioluminescence imaging is a technique that has been utilized to monitor cell viability and gene expression in various *in vivo* applications. However, it has never been applied in an *in vitro* setting for the specific purpose of evaluating a cell-scaffold construct.

This research describes the design of flow perfusion bioreactor system suitable for bioluminescence imaging. In the first experimental chapter, the system was tested using MC3T3-E1 cells transfected with a constitutive bioluminescent reporter. It was found that bioluminescence imaging was possible with this system. In the second experimental chapter, MC3T3-E1 cells transfected with BMP-2 linked bioluminescence reporter were cultured by flow perfusion for a period of 11 days. Bioluminescence was detectable from the cells starting at day 4, while peaking in intensity between days 7 and 9. Further, it was also found that bioluminescence occurred in distinct regions within the scaffold. These results indicate that these strategies may yield information not available with current assays.

Author's Acknowledgements

I must start by acknowledging my committee. I am grateful to my advisor, Dr. Aaron Goldstein for providing me with technical guidance, support, and most importantly, for always laughing at my jokes. Surely he is a more patient advisor than most. I am grateful to Dr. Abby Morgan for use of her freeze drier and Dr. Ge Wang for use of his imaging equipment, as well as to both of them for serving on the committee.

However, such work is not accomplished with the assistance of the committee alone. There are many other individuals who have had an immense impact on my work, and I would like to take the space to acknowledge them here. First, my sincerest thanks to Dr. Haiou Shen for his work with the bioluminescent imaging system. He would always take the time to answer my questions, and I cannot express how much this project would have never been completed if he had not devoted his time and energy to it. Second, my sincerest thanks to Mike Vaught for his work on the bioreactor setup. His knowledge and creativity when approaching mechanical design made it possible to transform an abstract idea into a realized product. I would have never have been able to design such a system on my own.

I must also thank Eunna Chung for her help on the MTT assay, Saugata Sarkar for his help with characterizing the optical properties of my materials, Tyler Horseman for his assistance with the freeze drier, Matthias Hofman for the use of the PhotonMax camera and other technical advice, Robyn Shaffer for her help with mRNA isolation and other advice, Catherine Ward for her help with the sterilization of my scaffolds, Yeonhee Kim for her assistance with the plate reader assays, the students in Dr. Lee's lab for their assistance with their laboratory equipment, and Dr. Lindsay Bashur for teaching me impeccable technique for cell culture and for her work on developing the BMP-2-Luc reporter cell line. My best wishes to all of you in your professional endeavors.

I must thank my colleagues from the Goldstein and Morgan labs; in particular, Satya Samavedi, Paola Jaramillo, and Tyler Horseman, for your friendship, for your help in the lab, and for making my time at Virginia Tech bearable. Thank you all so much.

I must thank my parents for encouraging my interests in science at a young age; else I might have done something really stupid with my life, such as gone to law school.

Lastly, to my husband Hammad, the love of my life: I must thank you for supporting and believing in me, so that I could complete this degree.

Table of Contents

List of Figures

List of Tables

Chapter 1: Introduction

1.1 Significance

Disease, trauma, congenital defects, and age-related degeneration necessitate the need for bone replacements to restore function. Materials currently used for bone repair include autologous bone, allogeneic bone, and synthetics. Autologous bone, or bone derived from the same donor source as the transplant (in most cases, from the iliac crest), has been considered the gold standard for many years because it exhibits the same phenotypic response as the surrounding bone tissue and elicits no immune rejection [1]. Autologous bone has the capacity to guide normal bone healing and remodeling processes; however, limited availability and donor site pain and morbidity hamper a larger scale use of this source [1]. Allograft bone, or bone from cadaver sources, is another potential source for bone replacement, yet this source has its own limitations, including immune rejection, disease transmission, and decreased mechanical strength [2]. Synthetics have the advantages of an unlimited supply; however, they often suffer from poor integration and fatigue failure at the implant site [3].

Thus, researchers have endeavored to employ tissue engineering strategies to overcome the limitations of the current materials. In principle, tissue engineered bone would have the regenerative potential of autologous bone, but the availability of synthetics. A current strategy for the manufacture of a tissue engineered bone replacement of involves culturing osteoprogenitor cells in a biocompatible scaffold and then implanting the scaffold in the patient to stimulate repair of the tissue [3].

A successful functional bone tissue engineered replacement will exhibit the properties of bone that in part can be identified and characterized by the specific genes and proteins expressed by the cells. Additionally, the construct must exhibit certain mechanical properties and a mineral phase. To evaluate the ability of the replacement to exhibit these properties, the cell-scaffold construct must be analyzed for these specific genes, proteins and the existence of mineral deposition. However, many of the techniques employed for this analysis are destructive, making it impossible to monitor the development of functional replacement in a spatial and temporal manner. This introduction briefly covers the fundamental issues surrounding the development of a functional tissue engineered replacement for bone using the tissue engineering strategy, including an overview of bone biology and the specifics of implementing the tissue engineering

strategy for bone. It then introduces bioluminescence imaging and tomography as potential tools for evaluation of cell-scaffold constructs.

1.2 Bone Biology

Bone tissue engineering is a complex problem in part due to the composite makeup of bone. Bone, as an organ, consists of mineralized tissues and blood vessels, nerves, marrow, and cartilage. The components of mineralized bone tissue include cells, collagenous and noncollagenous proteins (organic component), and an inorganic mineral component [4]. These components together give bone its mechanical strength and other biological and chemical properties for appropriate bone function [4]. The components are discussed below.

1.2.1 Cell Types

There are three predominate cell types in bone: osteoblasts, osteocytes, and osteoclasts. Osteoblasts and osteocytes are the cells that originate from mesenchymal stem cell lineage [4]. Osteoblasts are the cells responsible for the production of bone matrix. Once bone matrix has been produced, osteoblasts can inactivate and become osteocytes. Osteocytes are embedded in bone and play a role in the mechanosensory capabilities of the organ [5]. Osteoclasts, which are derived from the hematopoetic lineage, are the cells that resorb bone [4]. Osteoblasts and osteoclasts work in concert with each other to govern the body's natural bone remodeling process [4, 6].

1.2.2 Proteins and other Organic Components

Around 20 percent by weight of bone is made up of protein and other organic components [4]. Several important extracellular matrix and non-extracellular matrix proteins are listed in Table 1.1.

ECM proteins:[4, 5, 7]	
Collagen1α1	The main structural component of bone ECM
Decorin	Also known as bone proteoglycan II, involved in ECM organization
Osteonectin	A phosphorylated glycoprotein; binds to calcium, and involved with cell spreading and possibly osteonectin
Osteopontin	A phosphoprotein that assists with cell attachment via RGD sequence, binds to hydroxyapatite; assists with cell attachment to bone matrix
Bone sialo protein	A phosphoprotein that binds to cells and hydroxyapatite through RGD sequence; assists with cell attachment to bone matrix
Osteocalcin	Binds Ca^{2+} and to hydroxyapatite, contains gamma carboxyglutamic acid, vitamin D responsive, involved in mineralization, involved in osteoclast recruitment/differentiation
Others:[5, 7]	
Alkaline phosphatase	An enzyme involved in promoting mineralization by removing nucleation inhibitors
BMP-2, -4, -7	Members of TGFβ family, induces bone formation *in vivo* by stimulating proliferation and differentiation of osteoblasts

Table 1.1 Important bone matrix proteins.

In particular, bone morphogenetic proteins (BMPs) have been considered particularly important in stimulating new bone formation, and BMP-2 and -7 are approved for use by the FDA in clinical trials [8, 9]. BMPs have also been used in bone tissue engineering applications [10-14].

1.2.3 Inorganic Component

The inorganic component of bone, which is 65 percent of the weight of bone, is composed of calcium, phosphate, carbonate, sodium, and magnesium. The mineral is formed as

a weak hydroxyapatite [4]. The inorganic component allows for bone to serves as a source of calcium and phosphate ions for the blood [4].

1.3 Tissue Engineering Strategy for Bone

The tissue engineering strategy aims to create functionalize tissue replacements by integrating engineering and biological concepts [15]. A successful implementation of the tissue engineering strategy for bone should yield a bone-graft substitute that is osteoconductive, osteogenic and osteoinductive [1]. Osteoconduction refers to when the bone-graft substitute allows for the in growth of new cells from the surrounding host tissue [16]. Osteogenesis refers to the formation of new bone from the cells implanted with the bone-graft substitute [16]. Osteoinduction refers to when the substitute allows for the active recruitment of osteoprogenitor cells from the surrounding host tissue [17]. Specific *in vitro* culture conditions, often in a bioreactor, may lead to the production of an extracellular matrix that may promote osteogenesis, osteoconduction and osteoinduction as opposed to a scaffold alone. The specific components to the tissue engineering strategy as applied to bone are discussed below.

1.3.1 Osteoprogenitor Cells

In accordance with the cellular biology of bone, osteoprogenitor cells are used in bone tissue engineering applications. They are generally highly proliferative and have the capability to differentiate to the osteoblastic phenotype [18]. There are three distinct stages in which this differentiation process occurs. First, osteoprogenitor cells undergo a proliferation stage, marked by a rapid increase in cell division. Next, the cells begin to develop and mature an extracellular matrix, marked in part with the production of type I collagen. Last, the cells begin to mineralize the matrix and eventually differentiate to osteoblasts.

From a clinical perspective, mesenchymal stem cells are the most compatible source for osteoprogenitor cells. Mesenchymal stem cells are highly proliferative and have the ability to differentiate into multiple cell types, including osteoblasts, adipocytes, and chrondrocytes [18]. However, for model studies, cell lines can be used. The advantage to using cell lines over primary cells is that the experiments conducted in cell lines can be compared equally without the batch to batch variation with primary cells. In particular, the MC3T3-E1 cell line is commonly

used for *in vitro* studies. The MC3T3-E1 line is a mouse osteoprogenitor cell line that was derived from mouse calvarial bone [19].

1.3.2 Scaffolds

A biocompatible scaffold in which to culture cells is a vital component of the tissue engineering strategy. The scaffold serves as structural support for cell attachment during initial stages of *in vitro* culture and provides a structure to fill the critical size defect. Scaffold materials can be classified as metals, ceramics, and polymers (or some combination of the three) [20]. The most commonly used materials for scaffolds are polymers, which can further classified by synthetic or natural origin. Synthetic polymers, such as polyurethane, poly-lactic acid, and polycaprolactone, generally provide sufficient mechanical strength and can be engineered to have a desired degradation rate [20]. A number of biocompatible scaffolds can be fabricated from naturally derived materials, including chitosan, collagen, alginate, starch, hyaluronic acid, and gelatin [21-26]. When compared to other materials, naturally derived materials are likely the closest mimics for the native cellular environment; however, they generally do not have the mechanical properties required for transplantation [20]. Both synthetic and natural materials can be fabricated into three dimensional scaffolds with techniques such as solvent casting/particulate leaching, rapid prototyping techniques, electrospinning, and supercritical fluid processes; among others [27]. The processing techniques generally depend on the material type and the desired architecture. The biomaterial may be engineered to release certain pharmaceutics into the system, ranging from growth factors (BMPs [12, 13] and transforming growth factor (TGF)-β1 [14]) to hormones (dexamethasone [28] and parathyroid hormone [29]). These pharmaceutics may provide for more directed differentiation of the cells.

1.3.3 Bioreactor system

Bioreactors are employed for *in vitro* culture of cell-scaffold constructs. The purpose of the bioreactor is to maintain the appropriate pH, oxygen, mechanical stimulation, pharmaceutics delivery and nutrient supply to the scaffold to allow for the desired proliferation and differentiation of the cells [30]. Delivery of these factors in a large construct is important since diffusion is only an effective means of transport for only a 100-200 μm depth into the scaffold [30]. For bone tissue engineering, perfusion bioreactors not only increase nutrient transport but

also have shown to stimulate differentiation and mineralization [31]. Bone cells appear to respond to both mechanical strain and fluid flow [5, 23, 32].

1.4 Evaluation of Tissue Engineered Constructs

To determine if a cell-scaffold construct has the certain functional qualities for bone repair, a number of assays are employed. To address cell viability and proliferation, assays that bind to either DNA, such as Picogreen™ [33] or bisbenzimidazole (Hoechst 33258) [34] fluorescent dyes, or assays that interact with the cell mitochondria, such as 3-(4,5-dimethylthiazol-2-yl)-2,5-diphenyltetrazolium bromide (MTT) [35] or 3-(4,5-dimethylthiazol-2-yl)-5-(3-carboxymethoxyphenyl)-2-(4-sulfophenyl)-2H-tetrazolium (MTS) [36], are used. To evaluate gene expression or for the presence of proteins, assays such as reverse transcription-polymerase chain reaction (RT-PCR), enzyme-linked immunosorbant assay (ELISA), or immunohistochemical staining are employed. For example, Gomes 2006 performed histological analysis and immunostaining on bone marrow stromal cells seeded on starch scaffolds that had undergone flow perfusion for up to sixteen days [37]. They found that it was possible to identify localized areas that stained positively for factors including BMP-2, vascular endothelial growth factor (VEGF), fibroblast growth factor (FGF)-2, and TGF-β1.

Imaging techniques such as x-ray computed tomography can reveal information in a nondestructive manner about the structure of the scaffold, and biological function may be deduced from this structural information [38, 39]. For example, the structure of the scaffold may yield information about the interconnectivity of the pore spaces or the development of a mineralized phase. However, x-ray computed tomography does not reveal direct information about specific biological function of the cell-scaffold construct.

1.5 Bioluminescence Imaging

In vivo imaging of cell proliferation and viability often involves utilizing the photonic properties of bioluminescent or fluorescent proteins [40]. Bioluminescence imaging relies on transfection of cells with luciferase enzymes (or other bioluminescent proteins), and upon addition of luciferin substrate, the following reaction occurs: [41]

$$luciferase + luciferin + ATP \xleftrightarrow{Mg^{+}} luciferase \cdot luciferyl - AMP + PP_i$$
$$luciferase \cdot luciferyl - AMP + O_2 \rightarrow luciferase + oxyluciferin + AMP + CO_2 + h\nu$$

The energy emission generally occurs in the visible range. Thus, optical imaging systems are employed to monitor cellular activity. Current applications of bioluminescence imaging include monitoring of gene expression, tumor metastasis, infection, and cytotoxicity [40].

1.5.1 Bioluminescent Reporters

There are several types of bioluminescent reporters based on the origin of the protein itself. The most common reporter is firefly luciferase, which is isolated from *Photinus pyralis.* Firefly luciferase has an peak emission wavelength of 612 nm at 37ºC [42]. Another common reporter is *Renilla* luciferase, which is isolated from sea pansy. It utilizes the colenterazine substrate and Ca^{2+} as a cofactor [43]. The wild-type *Renilla* has an average emission wavelength of 460-490 nm [43, 44]. Luciferase reporters can also emit at a different wavelengths without significant changes to the fundamental biochemical reaction with small genetic changes in the encoding DNA [45]. Thus, there is the potential to use multiple luciferase reporters to study multiple biological processes in one setting.

1.5.2 Applications of Bioluminescence Imaging to Tissue Engineering

1.5.2.1 In vivo Animal Models

Bioluminescence imaging has only recently begun to be utilized for tissue engineering applications, in large part due to the non-destructive nature in evaluating cell viability. The work has mostly revolved around the *in vivo* imaging of cell-scaffold constructs in animal models. The first experiments to develop a luciferase-expressing cell line for use with in tissue engineering applications was published in 2004, when Blum 2004 transfected CRL-1764 cells (rat fibroblasts) to express an enhanced GFP-luciferase vector [46]. These cells were seeded onto titanium meshes and implanted subcutaneously into Fisher 344 rats. For the 28 day period of the study, the animals were imaged with bioluminescence imaging upon injection with D-luciferin. While the authors report that while they were able to ascertain the location of the implants by bioluminescence imaging, they reported wide variability of signal from the implants.

Nevertheless, this study opened up the possibility to using bioluminescence imaging to monitor cell viability in tissue engineering applications.

The *in vivo* studies that have followed have used bioluminescence imaging to explore different aspects of the tissue engineering strategy, be it the cell type, scaffold material, or other aspect. Roman 2007 used three different types of hydrogels as scaffold materials with C3H/10T1/2 luciferase-GFP transfected cells to monitor cell proliferation in subcutaneous and intramuscular implants in BABL/c homozygous nude mice [47]. Using bioluminescence imaging upon injection of the substrate D-luciferin, cell viability was detected at the scaffold sites for up to three months *in vivo*; although, they reported better cell proliferation at the intramuscular sites as compared to the subcutaneous sites. Degano 2008 compared the ability of bone marrow and adipose-derived mesenchymal stem cells for use in bone repair [48]. They transfected both cell types, seeded them onto hydrogel scaffolds, and implanted in a defect in the calvarial bone into BALB/c homozygous nude mice. They found, as demonstrated by bioluminescence imaging, that bone marrow mesenchymal stem cells had a better survival rate. Vilalta 2009 observed the expression of a collagen promoter in an attempt to monitor chondrogenic differentiation of both CR1 and adipose-derived mesenchymal stem cells [49]. They transfected these cells with type II procollagen promoter-luciferase reporter, seeded them onto demineralized bone matrix scaffolds, and implanted subcutaneously into SCID mice. The mice were imaged at various time points during the study period of six weeks. The resulting bioluminescent images of the promoter from the implants correlated with the subsequent immunohistochemical analysis of the implant site, indicating that areas of the scaffolds that expressed the reporter also stained for type II procollagen.

1.5.2.2 In vitro Studies

Even more recently, this type of work has been expanded to monitoring *in vitro* bioreactor systems. Liu 2009 describes the first flow perfusion bioreactor application [50]. The authors used a hypoxia response element–luciferase (HRE-Luc) to study O_2 availability throughout a tissue engineered scaffold undergoing flow perfusion. The transfected cells were seeded onto tri-β calcium phosphate particles and cultured either at 5% or 20% O_2 in a flow perfusion bioreactor. Over the course of four days of culture, the luciferase activity for the 5%

O_2 was higher than in the 20% O_2, indicating a more hypoxic environment. However, they did not attempt to localize the location of the bioluminescence *in vitro*.

1.6 Bioluminescence Tomography

1.6.1 Theory

Bioluminescence imaging, while informative, does not involve quantitative localization of cellular activity because it does not account for photon propagation throughout the biological tissue [51]. In particular, it is hampered by both the limits of the penetration depth of the light photons and by the limited spatial resolution due to photonic scattering behavior in the tissue [52]. Thus, it only provide relative quantitative information in a two dimensional planar domain. Bioluminescence tomography is now employed to quantitatively reconstruct the *in vivo* light source (and thus the cellular activity). One technique for the reconstruction is based on the finite element model of the three-dimensional steady-state diffusion approximation to the radiative transport equation, shown in Equation 1.1:

$$\begin{cases} -\nabla \cdot (D(\vec{x})\nabla\Phi(\vec{x})) + \mu_a(\vec{x})\Phi(\vec{x}) = S(\vec{x}) \\ D(\vec{x}) = (3(\mu_a(\vec{x}) + \mu_s(\vec{x})))^{-1} \end{cases} \tag{1.1}$$

where μ_a and μ_s are the absorption and scattering coefficients, or probability of photon absorption or scattering per unit distance [mm^{-1}], respectively, Φ is the photon density [$Watts/mm^2$] at location x, and S is the source density [$Watts/mm^3$]. The diffusion approximation can apply to bioluminescent photons *in vivo* since scattering is outpaces absorption in biological tissue [53, 54]. The absorption and scattering coefficients are material dependent and determined by experimentation [51, 53].

1.6.2 Finite Element Model

In order to reconstruct the bioluminescent signal, the estimation of the source is made and the forward diffusion equation is solved. The linear model is given in Equation 1.2.

$$([K]+[C])(\Phi) = [S] + \beta \tag{1.2}$$

The matrices are given in Equation 1.3:

$$\begin{cases} K_{ij} = \int_{\Omega} D(\nabla \psi_i(\vec{x})) \cdot (\nabla \psi_j(\vec{x}))\, d\Omega \\ C_{ij} = \int_{\Omega} \mu_a \psi_i(\vec{x}) \psi_j(\vec{x})\, d\Omega \\ S_j = \int_{\Omega} S(\vec{x}) \psi_j\, d\Omega \\ \beta_j = \int \psi_j(\vec{x}) \Gamma(\vec{x})\, d(\partial\Omega) \end{cases} \tag{1.3}$$

where ψj is the interpolation function over the domain, Ω. The photon density is discretized in Equation 1.4.

$$\Phi(\vec{x}) = \sum_{k=1}^{D} \Phi_i(\vec{x}) \psi_i \tag{1.4}$$

The error between the actual image and estimation is minimized using various regularization techniques [53].

1.6.3 In vivo Tumorgenesis Model

The first *in vivo* bioluminescence tomography experiments were reported in 2006, which detailed the reconstruction efforts to study tumorgenesis in mice [54]. Briefly, a mouse was injected with luciferase-expressing human prostate cancer cells. To observe the growth of a tumor over time, the mouse was anesthetized and injected with D-luciferin. The mouse was then imaged on the anterior, right lateral, posterior and left lateral views with a CCD camera. At the termination of the experiment, the mouse was then sacrificed and dissected to determine the specific size and location of the tumors.

In this particular case, two different tumors grew superior to each adrenal gland. The bioluminescent output of each tumor did not correlate with the relative tumor size. The authors note that this difference may be attributed to volume of non-viable cells within the overall tumor volume. Even so, the authors were able to predict the location of the tumor by bioluminescence tomography and verify such by dissection.

1.7 Conclusions and Motivation for the Current Work

The applications of bioluminescence imaging for to tissue engineering applications have not been fully explored. There are two specific objectives addressed in this thesis. The first objective, as described in Chapter 2, is the design and construction of a flow perfusion bioreactor in which bioluminescence imaging and tomography can be applied for non invasive *in vitro* detection and monitoring of bioluminescence reporters. The second objective, as described in Chapter 3, is to apply the bioreactor system to monitor the expression of BMP-2 in MC3T3-E1 cells undergoing flow perfusion by bioluminescence imaging.

The intention is to advance the field by developing imaging and tomographic protocols for further advanced applications of this technology *in vitro*. The bioreactor system is not only appropriate for bone tissue engineering strategies, but also is a potential model system, with a simple geometry, for the implementation of imaging protocols. With implementation of these imaging strategies, this technology has the potential to yield real-time information about the development of tissue-engineered constructs not available with current assays.

Chapter 2: The Design and Construction of a Flow Perfusion Bioreactor Suitable for Bioluminescence Imaging

Sarah J. Lapp[1], Haiou Shen[1,2], and Aaron S. Goldstein[1,3]

1. School of Biomedical Engineering and Sciences
2. Biomedical Imaging Division
Virginia Tech-Wake Forest University

3. Department of Chemical Engineering
Virginia Polytechnic Institute and State University

2.1 Introduction

Bioluminescence imaging has been shown to be a promising tool for the non-destructive evaluation of cells *in vivo*. Applications of bioluminescence imaging include tumorgenesis models [55, 56], infection monitoring [57, 58], and gene delivery [59, 60]. Recently, bioluminescence imaging has been utilized in tissue engineering applications to monitor cell viability and gene expression *in vivo* [48-50, 61]. With any imaging modality, the intrinsic challenges such as photon absorption and scattering throughout the tissue must be addressed in quantifying and reconstructing the image source [62]. Bioluminescent imaging is no exception, and thus these previous studies are largely qualitative in nature. The ability to noninvasively measure and quantify cell viability and gene induction in large tissues would make it possible for the monitoring of tissue development and healing over time.

Bioreactors are employed for *in vitro* culture of cell-scaffold constructs. The purpose of the bioreactor is to maintain the appropriate pH, oxygen, mechanical stimulation, pharmaceutics delivery and nutrient supply to the scaffold to allow for the desired proliferation and differentiation of the cells. For bone tissue engineering, perfusion bioreactors have shown to stimulate differentiation and mineralization *in vitro* [31]. However, due to the destructive nature of assays necessary to evaluate the cell-scaffold construct, evaluation of cell viability and gene expression in a spatial and temporal manner is difficult.

The overall goal of this study is to design and construct a bioreactor suitable for flow perfusion and optical imaging. The specific challenges that were addressed were the design and construction of bioreactor with the appropriate shape and size, the ability of a transfection

procedure to produce bioluminescence cells, and the ability of these cells to be detected in various optical media. Two types of materials were selected to image in: gelatin, which was cast as a transparent gel, and chitosan, which was fabricated into a porous, translucent scaffold. The gelatin was designed to be a simpler test of the ability of the system to image small numbers of cells. The porous chitosan was designed to be more representative of scaffold materials for tissue engineering applications. However, the suitably of the translucent chitosan for use with bioluminescence imaging had to be addressed.

2.2 Materials and Methods

2.2.1 Bioreactor and Perfusion Flow Loop

The bioreactor chamber, Figure 2.1, was fabricated out of PMMA rectangular slabs. The dimensions of the bioreactor were 13 × 13 × 25 mm, with 12 mm-thick walls. Rectangular pieces were chosen to provide a flat edge for clear imaging. PMMA has been shown to be non-toxic to cells and has been used in the laboratory for previous bioreactor setups [63]. A scaffold is cut to the inner dimensions of the bioreactor and placed inside for static or perfusion culture. The top and bottom of the bioreactor was affixed with a top and bottom plate and sealed with Viton 119 O-ring (MSC Industrial Supply, Melville, NY). The perfusion flow loop was based on the previous designs in the lab [64, 65]. The schematic of the system is shown Figure 2.1 and the actual system is shown in Figure 2.2. It is composed of a Masterflex Digital Console Drive, model 7519-05 (Cole-Parmer, Vernon Hills, Il) to drive the fluid flow, a flow meter to measure the fluid flow, a glass reservoir to hold culture media, and the bioreactor chamber.

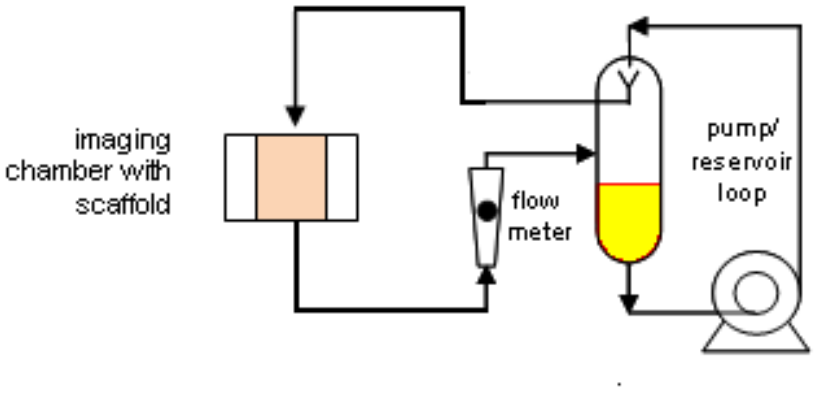

Figure 2.1 – Flow perfusion schematic.

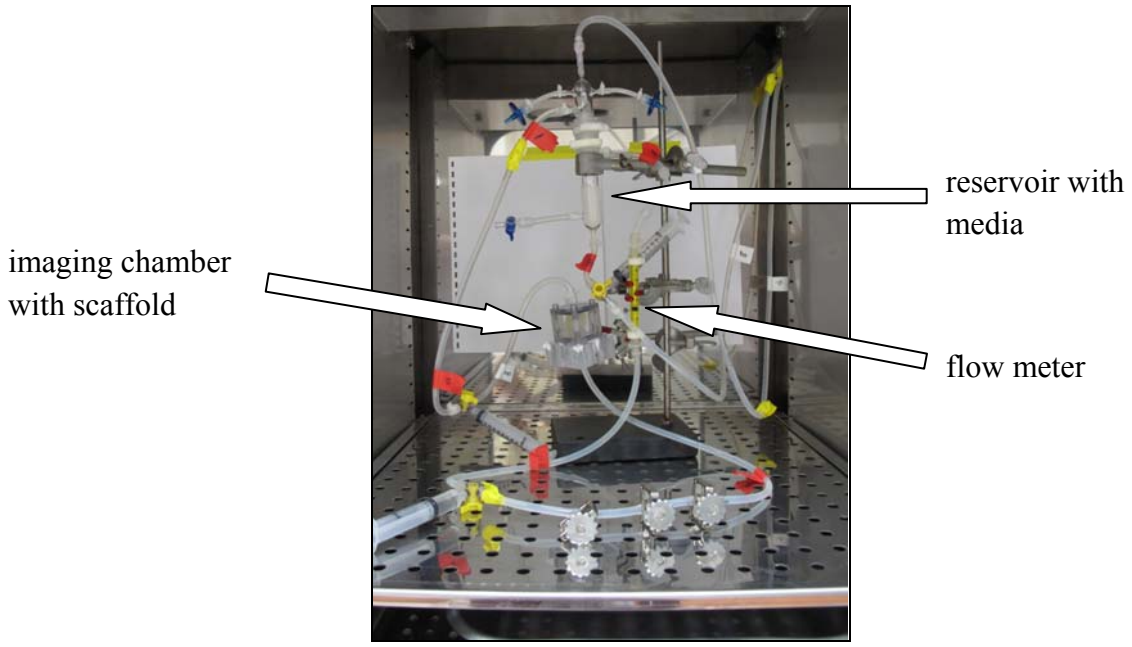

Figure 2.2 – Flow perfusion setup.

2.2.2 Imaging Setup

The imaging setup, shown in Figure 2.3, is based on the setup used for the mouse model bioluminescence tomography experiments previously performed [54]. The setup is composed of a VersArray 2048B charged couple device camera (Princeton Instruments, Trenton, NJ) to capture the images, and a PRM1Z71 motorized rotation stage (Thorlabs, Newton, NJ) in which to mount and align the bioreactor. The VersArray 2048B camera has a 2048×2048 imaging array with a 13.5×13.5 μm pixel size. The images were collected under 2×2 hardware binning and the camera detector temperature was maintained at -110°C with liquid nitrogen. The camera lens, with attached extender, was placed 82 mm from the outer edge of the bioreactor. The entire imaging setup was contained in a black felt-covered enclosure to prevent outside light photons from being detected by the camera. The images were captured and processed with Win32 software (Princeton Instruments), and further processed with Matlab (Mathworks, Natick, MA). The rotation stage was controlled with APT software (Thorlabs).

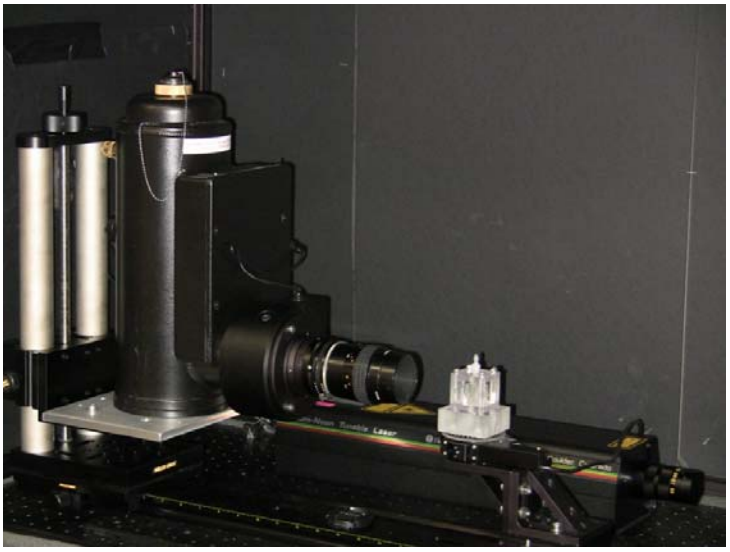

Figure 2.3 Imaging system. Princeton Versarray 2048B CCD camera (left) and bioreactor (right) housed in a dark box.

2.2.3 Cell Culture and Transfection

MC3T3-E1 cells were cultured in alpha-MEM (Invitrogen, Carlsbad, CA) plus 10% fetal bovine serum (Gemini BioProducts, West Sacramento, CA) and 1% antibiotic/antimycotic (Mediatech, Manassas, VA) and passaged before confluency. To produce light-emitting cells, MC3T3-E1 cells were transiently transfected with pRL-SV40 reporter gene (Promega, Madison, WI) using the transfection reagent Lipofectamine^{TM} 2000 (Invitrogen). The pRL-SV40 reporter gene, shown in Figure 2.4, contains Renilla luciferase (RLuc) cDNA and is a constitutive reporter; thus it is a marker of cell viability. The RLuc acts on colenterazine substrate and produces light at 480 nm. Lipofectamine^{TM} 2000 is a cationic lipid-mediated transfection reagent that allows for delivery of the foreign DNA through the cell membrane.

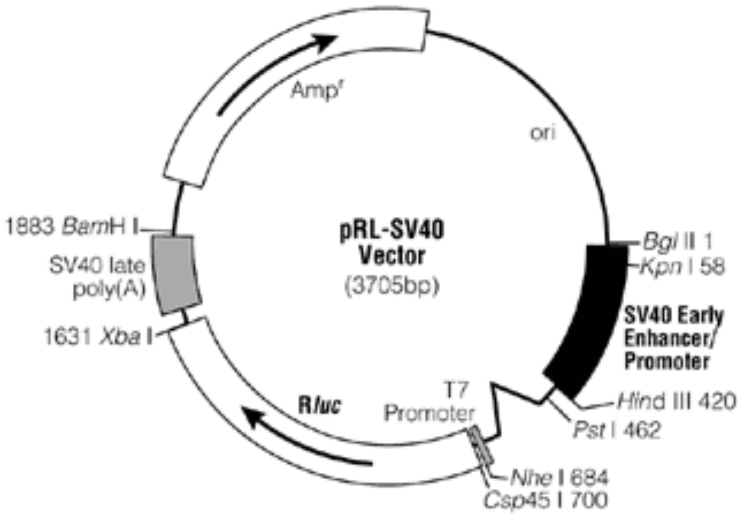

Figure 2.4 pRL-SV40 vector.

To perform the transfection, 2 μL of pRL-SV40 in 200 μL of α-MEM and 2 μL of Lipofectamine^{TM} 2000 in 200 μL of α-MEM were incubated separately for 5 minutes. The solutions were then combined and incubated together for 20 minutes at room temperature. Then, the cells (at 60-80% confluency) were cultured with the transfection solution in an additional 3 mL of α-MEM for 4-6 hours, and then cultured in α-MEM plus 10% FBS and 1% antibiotic/antimycotic for a rest period of 24 hours. The imaging was performed within 48 hours of transfection.

2.2.4 Phantom Preparation and Evaluation

To evaluate the ability of the system to detect bioluminescent cells, both transparent (gelatin blocks) and semi-transparent (chitosan scaffolds) phantoms were prepared and imaged. Gelatin blocks were created by dissolving 1 g of porcine gelatin (Sigma, St. Louis, MO) in 9 grams of water for a total of 10 g. The gelatin was allowed to sit for 10 minutes and then gently agitated at 37°C for at least 30 minutes or until dissolved. The resulting solution was then cast in a 12 well plate and allowed to cool for 10 minutes. Then, approximately 25 μL of air was injected into the block to form a void space. The gelatin was stored overnight at 4°C. Before imaging, the gelatin was cut to fit into the bioreactor.

Chitosan scaffolds were prepared by dissolving 2% (by weight) chitosan (Sigma) in 1% (by volume) acetic acid for a minimum of 48 hours under agitation. The solution was cast into

50 mL centrifuge tubes and frozen at -20° C for at least 12 hours, and then lyophilized for 48-72 hours. The scaffolds were then cut to the dimensions of the bioreactor, washed with 1 M NaOH to neutralize the residual acetic acid and then washed repeatedly with DI water to remove the residual base.

The absorption and scattering coefficients of the porous chitosan were determined by spectrophotometry. This evaluation was to determine if chitosan had similar optical properties to that of biological tissue. A 2 mm-thick piece of chitosan scaffold was incubated with phenol red-free eagle MEM (Sigma) and sandwiched in between two glass slides. The percent transmission and reflectance from the sample was measured between 200 and 1200 nm with a Cary 5000 UV-Vis-NIR spectrophotometer with a DRA-2500 diffuse reflectance accessory (Varian, Palo Alto, CA). The absorption and scattering coefficients were determined by the inverse adding-doubling method [66].

2.2.5 Imaging

2.2.5.1 Bioluminescence Imaging in Gelatin

To image cells in the gelatin gels with bioluminescence imaging, transfected cells were combined with colenterazine substrate (Promega). The colenterazine (CoE) stock solution was composed of 250 μg of CoE diluted in 125 μL of 100% ethanol. Cells were enzymatically lifted with 1X trypsin/EDTA (American Type Cell Culture, Manassas, VA), counted, and made into a cell suspension with eagle phenol red-free MEM (Sigma) of 1.5 million cells/mL. This suspension was combined with working CoE solution, which was composed of 20 μL of CoE stock solution in 2 mL of phenol red-free eagle MEM, for a final concentration of 20 μg/mL of substrate. The cell suspension/CoE solution was injected into void space, and the gel was placed in the bioreactor for imaging. Each face of the bioreactor was imaged under brightfield and then correspondingly imaged with bioluminescence imaging for 5 minutes, f/1.2.

2.2.5.2 Bioluminescence Imaging in Chitosan

To image cells in the chitosan scaffolds, the cells were enzymatically lifted and made into a cell suspension with eagle phenol red-free MEM of 250,000 cells/mL. The scaffolds were seeded with 200 μL of the suspension (approximately 50,000 cells) by injection and incubated

over night to allow the cells to attach. The scaffold was then incubated with 7 μg/mL CoE working solution, placed in the bioreactor, and imaged. Each face of the bioreactor was imaged under brightfield and then correspondingly imaged with bioluminescence imaging for 5 minutes, f/1.2. The signal was reconstructed by use of a simple signal mapping algorithm.

2.2.5.3 Bioluminescence Imaging of a Point Source in Chitosan

To create a point source for imaging in a chitosan scaffolds, cells were combined with alginate and formed into a bead. Alginate (Sigma) was weighed, placed in a centrifuge and sterilized by UV light over night. The alginate was then dissolved in phosphate buffer saline (Mediatech, Manassas, VA) to make a 3.6 % (by weight) alginate solution. The cells were enzymatically lifted with 1X trypsin/EDTA, counted, and made into a 350,000 cells/mL suspension with phenol red-free eagle MEM. The beads were prepared by combining 2 parts alginate with 1 part cell suspension. Then, the alginate-cell mixture was extruded dropwise through an 18 gauge needle into .318 M $CaCl_2$ solution and allowed to gel for a few minutes. The beads, which were about 2 mm in diameter and contained approximately 1400 cells each, were washed with phosphate buffered saline and cultured in eagle phenol red-free MEM until imaging.

To determine if the cells were expressing the pRL-SV40 vector in the beads (thus producing light), the beads were placed in the wells of 96 black well plate with 1 μL/mL CoE working solution and imaged using the LAS-3000 Intelligent Darkbox (Fujifilm, Tokyo, Japan) under the chemiluminescence setting, ultra sensitivity (16x8 binning), tray setting 1, for 10 minutes.

To image the beads in the scaffolds in the bioreactor, pieces of chitosan were cut into 6 mm thick pieces (Figure 2.5). A bead was then wedged in between the chitosan scaffolds, incubated in working CoE solution, and placed in the bioreactor for imaging. Each face of the bioreactor was imaged under brightfield and then correspondingly imaged with bioluminescence imaging for 5 minutes, f/1.2.

Figure 2.5 Chitosan scaffolds and alginate beads.

2.3 Results

2.3.1 Determination of Optical Coefficients of Chitosan

The percent transmission and reflectance of porous chitosan were determined by spectrophotometry as described in Section 2.2.4. The spectra are shown in Figure 2.1.

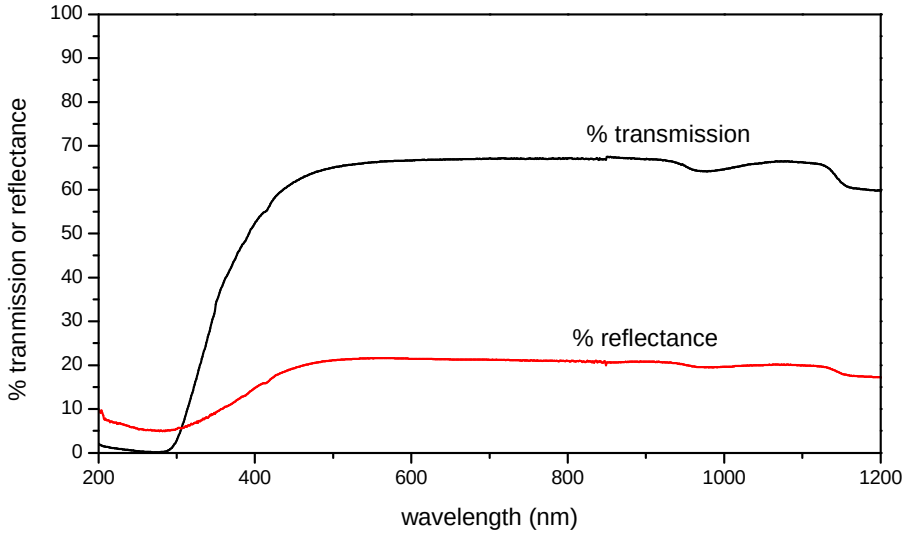

Figure 2.6 Percent transmission and reflectance of porous chitosan.

These spectra were used to compute the optical coefficients of porous chitosan by the inverse adding-doubling method. The computed coefficients for 480 and 615 nm are shown in Table 2.1

Wavelength (nm)	μ_a (mm^{-1})	μ_s' (mm^{-1})
480	0.011	0.135
615	0.008	0.130

Table 2.1 Optical coefficients for porous chitosan.

2.3.2 Bioluminescence Imaging in Gelatin

Cells were imaged in the gelatin phantom as described in Section 2.2.5.1. Figure 2.7 shows the four brightfield and four corresponding BLI images.

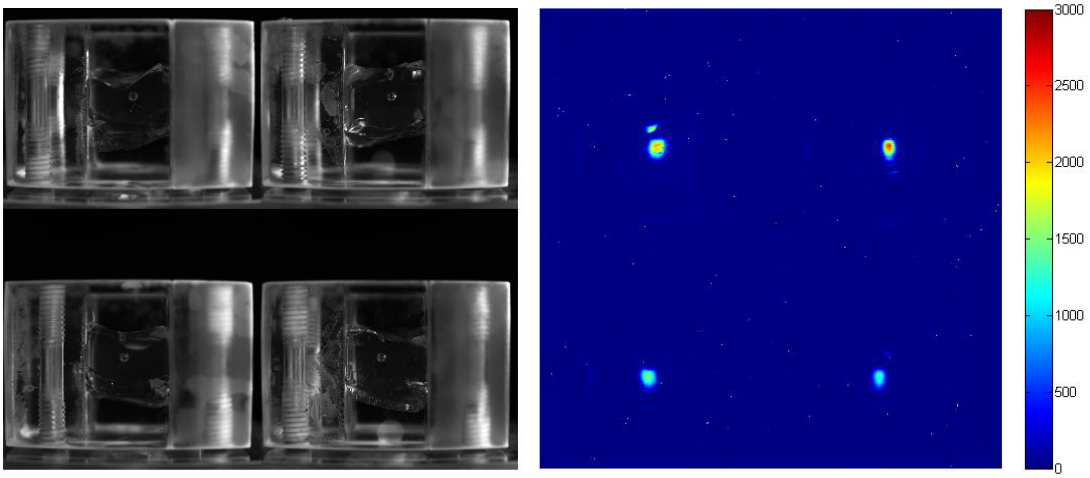

Figure 2.7 Brightfield (left) and bioluminescence (right) images of cells in gelatin. Bioluminescent images are false color. Scale bar is photons per pixel.

In the transparent gelatin, the bioluminescent signal is clearly defined within the boundaries of the void space where the cells were injected. The three dimensional source was easily reconstructed with a reconstruction algorithm as shown in Figure 2.8

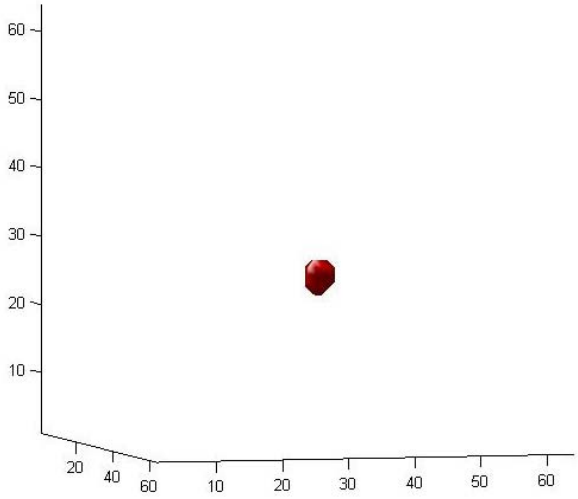

Figure 2.8. Reconstructed bioluminescence signal in gelatin.

2.3.3 Bioluminescent Imaging in Chitosan

Cells were imaged in the chitosan phantom as described in Section 2.2.5.2. Figure 2.9 shows the four brightfield and four corresponding BLI images.

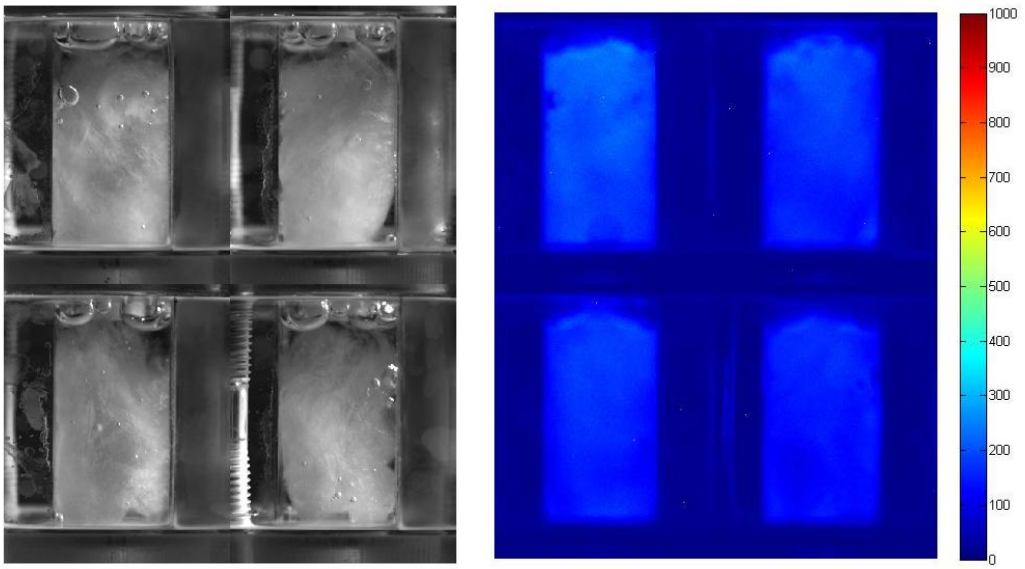

Figure 2.9. Brightfield (left) and bioluminescence (right) images of chitosan seeded by injection. Bioluminescence images are false color. Scale bar is photons per pixel.

2.3.4 Bioluminescence Imaging of a Point Source in Chitosan

The expression of pRL-SV40 vector in the alginate beads was confirmed by imaging the beads in the Intelligent Darkbox as described in Section 2.2.5.3. Figure 2.10 shows the image of the beads.

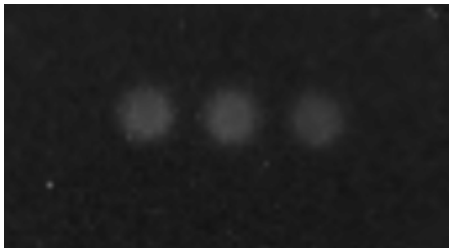

Figure 2.10 Expression of pRL-SV40 in alginate.

The alginate point source in the chitosan scaffold was then imaged by bioluminescence imaging as further described in Section 2.2.6.3. Figure 2.11 shows the four brightfield and four corresponding bioluminescence images.

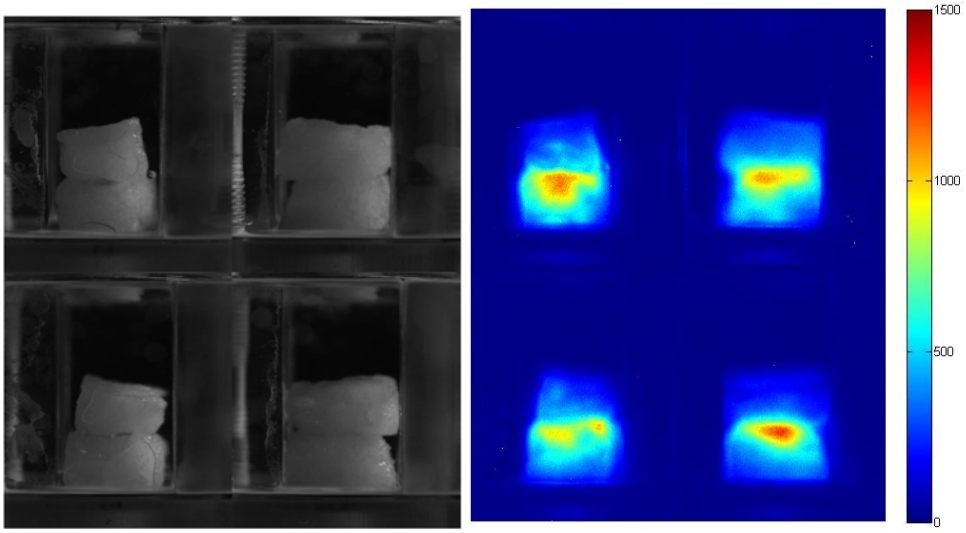

Figure 2.11 Brightfield (left) and bioluminescence (right) images of chitosan with embedded alginate point source. Bioluminescence images are false color.
Scale bar is photons per pixel.

2.4 Discussion

A number of different experiments were conducted to evaluate the feasibility of this system for bioluminescence imaging. First, chitosan had to be evaluated as an optically suitable material. This task was accomplished by determining the absorption and scattering coefficients

of the scaffold material by spectrophotometry. These coefficients represent the probability that a light photon will encounter an absorption or scattering event over a set distance; the higher the coefficient, the more likely such an event will occur. If the absorption coefficient is too high, the photons will not be detectable by the system. Thus, these coefficients reflect the effective thickness of a chitosan scaffold in which bioluminescence imaging is useful, particularly with low numbers of cells used for this work.

Based on the optical spectra of chitosan, the computed optical coefficients indicate that scattering outpaces absorption around 100 fold. These results can be compared to published data [67] on tissue and organs shown in Table 2.2.

	Muscle	Lung	Heart	Bone
μa (mm^{-1})	0.10	0.22	0.21	0.16
$\mu s'$ (mm^{-1})	1.20	2.30	2.00	1.28

Table 2.2 Representative optical coefficients of tissue.

Porous chitosan has less scattering and absorption as compared to tissue as defined by the optical coefficients. However, the ability to use spectrophotometry and inverse-adding doubling to determine the optical coefficients is hampered by the difficulty to control the path length of the sample. Particularly with porous chitosan, the thickness of the sample can change with a small amount of compression between the glass slides. Nevertheless, we believe the results to be a good guide for demonstrating that chitosan is optically suitable for this imaging-bioreactor system.

The next series of experiments were conducted to evaluate the ability of the system to perform bioluminescence imaging in the bioreactor. First, a low number of cells were imaged in a transparent gelatin phantom. This experiment was conducted to first observe if the transfection procedure was effective and to test the lower limit on the ability of this system to detect cells. The transparent gelatin was used so that little scattering and absorption the light photons would occur. Figure 2.7 showed that we were able to detect the cells at a point source in gelatin, indicating that the transfection was effective. With this result, we were able to use a simple algorithm to reconstruct the point source (Figure 2.8). The next experiments were conducted in chitosan scaffold. We imaged transfected cells seeded evenly throughout a chitosan scaffold and

found that at a low seeding density (50,000 cells/scaffold), bioluminescent signals were detectable (albeit weaker than in the gelatin).

The last imaging experiments involved imaging a bioluminescent point source embedded in a chitosan scaffold. Initially, we imaged the cell-encapsulated alginate to see if the cells would survive in the alginate and to see if colenterazine substrate would diffuse sufficiently throughout the alginate enough to produce sufficient bioluminescent signal (Figure 2.10). We then imaged the bead embedded in chitosan in the bioreactor (Figure 2.11). Bioluminescent signals were be not only considerably weaker than in the gelatin but also more diffuse; however, this result was expected when imaging in a more translucent material. Even so, the signal clearly originates from the center of the scaffold and is distinct from the areas with no cells.

In both Figures 2.7 and 2.9, the signal appears weaker in the fourth face of the bioreactor (bottom right) than in the first face of the bioreactor (top left). This difference may be due to the utilization of the substrate or the decrease in temperature. As this imaging occurred outside the incubator and took approximately 20 minutes, the temperature of the scaffolds and media certainly decreased from 37°C to room temperature. A change in temperature as been shown to shift the emission spectra of luciferase *in vivo* [68]. Additionally the sustained temperature decrease and time of culture outside the incubator may contribute to cell death, as conditions such as pH and O_2 content of the cell environment will not be maintained as compared to continuous culture in the incubator.

The contributions of these three factors (substrate utilization, temperature-based spectral shift, and cell death) to the decrease in signal may not be independently determined without significant experimentation and research. The development of a controlled imaging environment, with a sustained temperature of 37°C, may assist in this research, provided a heating system does not produce a significant amount of photonic noise.

The signal in Figure 2.11 does not follow the same trend from the first face to the fourth face. This result is presumably due to the placement of the alginate bead in the scaffold. While we attempted to place the bead at the center, it may have shifted when placing the construct in the bioreactor. Nevertheless, the signal does originate from a central location within the construct.

It may be possible to apply tomographic techniques to images like Figure 2.11; however, a number of changes must be made. First, optical properties of chitosan should be confirmed

with repeated experimentation. Second, the bead should be embedded with more cells to increase the signal intensity. Third, the scaffold should be formed in a shape that is more conducive to exact placement of the bead. With these steps, it may be possible to tomographically reconstruct the bioluminescent source.

2.5 Conclusions

We successfully designed and constructed a bioreactor system suitable for bioluminescence imaging, and tested it with low numbers of cells. Bioluminescence signal was detectable in both transparent (gelatin) and translucent (chitosan) media. Thus, this system may be useful in evaluating cell-seeded constructs.

2.6 Acknowledgements

The authors gratefully acknowledge Mike Vaught for his work on the design and construction of the bioreactor.

Chapter 3: Nondestructive Evaluation of BMP-2 Expression in a Tissue Engineered Construct in vitro by Bioluminescence Imaging

Sarah J. Lapp[1], Haiou Shen[1,2], and Aaron S. Goldstein[1,3]

1. School of Biomedical Engineering and Sciences
2. Biomedical Imaging Division
Virginia Tech-Wake Forest University

3. Department of Chemical Engineering
Virginia Polytechnic Institute and State University

3.1 Introduction

A common strategy for the development of a bone graft replacement is to culture stem cells on a biocompatible scaffold. However, current assays for evaluation of osteoblastic differentiation require damage or destruction of the construct. Therefore, it is difficult to monitor osteoblastic differentiation as a function of time and space.

The overall goal of this study is to noninvasively evaluate bone morphogenetic protein (BMP)-2 expression of MC3T3-E1 cells by bioluminescence imaging in a bioreactor. BMP-2 is thought to be a potent differentiation factor with respect to bone formation, and recombinant BMP-2 has been shown to stimulate ectopic bone formation when used in *ex vivo* gene therapy experiments [69]. BMP-2 has also been demonstrated to be highly localized in cell-seeded scaffolds undergoing flow perfusion [37]. The system described in Chapter 2 serves as a basis for the imaging techniques used in this chapter. The biomaterial used in this study is chitosan. Chitosan is a natural polysaccharide derived from the deacetylation of chitin from the exoskeletons of insects or crab shells. It has been widely researched as a scaffold material for tissue engineering applications and has been demonstrated to be biocompatible [22, 24]. Also, it has been demonstrated to be suitable for bone tissue engineering applications, and in particular, culture of MC3T3-E1 cells [70-73].

The first study in this chapter evaluates osteoblastic differentiation of MC3T3-E1 cells under static culture conditions in chitosan scaffolds. Using standard culture conditions, this study serves a basis of evaluating BMP-2 expression and osteoblastic differentiation of these cells as a function of the supporting biomaterial. The second study in this chapter correlates BMP-2 expression and luciferase activity in MC3T3-E1 cells that are stably transfected with a

BMP-2-luciferase reporter. This study is done concurrently with untransfected MC3T3-E1 cells in a monolayer culture to determine if there is a difference in BMP-2 expression due either the to the insertion of the luciferase reporter or the change in culture conditions. The third study in this chapter is the dynamic perfusion culture of the stably-transfected cells in a chitosan scaffold. The intent is to visualize the induction of BMP-2 within the scaffold, under perfusion flow, by imaging the expression of the luciferase reporter.

3.2 Materials and Methods

3.2.1 Cell Culture Materials and Transfection

Cells were grown in either alpha-MEM (Invitrogen) plus 10% fetal bovine serum (Gemini BioProducts) and 1% antibiotic/antimycotic (Mediatech, Manassas, VA), or phenol red-free eagle-MEM (Sigma) plus 10% fetal bovine serum and 1% antibiotic/antimycotic. The medias will be referred to as growth media and phenol red-free growth media, respectively.

For the differentiation studies, the cells were cultured in either growth media or phenol red-free growth media plus osteogenic supplements (2 mM L-ascorbic acid and 0.13 mM β-glycerolphosphate), and will be referred to as differentiation media and phenol red-free differentiation media, respectively. For the perfusion studies, the cells were cultured with phenol-red free differentiation media with 25mM HEPES buffer.

MC3T3-E1 cells were cultured in growth media and passaged before confluency. To create the bioluminescent reporter, MC3T3-E1 cells were stably transfected with BMP-2 Luc gene as previously described [74]. The transfected cells will be referred to as MB-Luc cells hereafter.

3.2.2 Scaffold Preparation

Chitosan scaffolds were prepared by dissolving 2% w/w chitosan in 1% v/v acetic acid for a minimum of 48 hours under agitation. The solution was cast either in a 15 mL or 50 mL centrifuge tube and frozen at -20° C for at least 12 hours, and then lyophilized for 48-72 hours. The scaffolds in the 15 mL centrifuge tubes were cut into 3mm discs for static 3D culture. The scaffolds in the 50 mL tubes were cut to the dimensions of the bioreactor (13 × 13 × 25 mm). The scaffolds were then washed with 1 M NaOH to neutralize the acetic acid and then washed

repeatedly with DI water to remove the residual base. Scaffolds were kept hydrated in phosphate buffered saline and sterilized by gamma-irradiation.

3.2.3 Static 3D Culture of MC3T3-E1 cells

To evaluate the effectiveness of chitosan as a scaffold material for bone tissue engineering, MC3T3-E1 cells were cultured in chitosan under static conditions for a period of 14 days. Cells were enzymatically lifted with 1X trypsin/EDTA (American Type Cell Culture, Manassas, VA), and scaffolds were seeded dropwise by pipette with 25,000 cells in a 100 μL suspension of growth media. Cells were allowed to attach for 1 hour before transferring the scaffolds to culture in differentiation media. Media was changed every 2 days.

3.2.3.1 Cell Viability in Static 3D Culture

Cell viability was determined by the 3-(4,5-dimethylthiazolyl-2)-2,5-diphenyl tetrazolium bromide (MTT) colorimetric assay at day 4. Scaffolds were washed twice with PBS to remove the culture media, removed from the culture dish, and incubated in 1 mL of working MTT reagent (.5 mg of MTT stock per mL phenol red-free eagle-MEM , MP Biomedicals, Solon, OH) for 4 hours. The reagent was then removed from culture and incubated under agitation for 15 in 1 mL of dimethyl sulfoxide (DMSO). The absorbance of the DMSO at 570 nm was measured using a Genesys 5 Spectronic spectrophotomer (Spectronic Analytical Instruments, Leeds, UK).

3.2.3.2 Alkaline Phosphatase Activity in Static 3D Culture

Alkaline phosphatase (ALP) activity was determined by colorimetric assay on days 7 and 14. Scaffolds were washed twice with PBS and placed in 990 μL of TGT buffer (50 mM Trizma HCL, 100 mM glycine, 0.1% Triton X100, pH 10.5) with 10 μL protease inhibitors (aprotinin, bestatin, leupeptin, E-64, and pepstatin A), and hand sonicated on ice before storage at -70°C. The samples were thawed and 100 μL of the supernatant was incubated with 500 μL of the ALP reagent (Biotron Diagnostics, Hemet, CA) at 30°C for 15 minutes. The reaction was then stopped with the addition of 500 μL of 0.3 M NaOH and the absorbance of 100 μL of each reaction was measured in duplicate by a SpectraMax M2 plate reader (Molecular Devices, Sunnyvale, CA) at 405 nm.

Alkaline phosphatase activity was defined as the rate of conversion of p-nitrophenol phosphate to p-nitrophenol, and the change in activity per minute is converted to alkaline phosphate concentration per minute (μmol/min) by Equation 3.1:

$$ALP\left(\frac{\mu mole}{\min}\right) = \Delta A / \min \times \frac{TSV}{\varepsilon \times LP \times SV} \times TV \tag{3.1}$$

where TSV is the total sample volume of 1.1 mL, ε is the absorptivity of p-nitrophenol (1.845×10^{-2} M^{-1} cm^{-1}), SV is the sample volume of 100 μL, TV is the total collection volume of 1 mL, and LP is the path length through the sample volume (0.33 cm for 100 μL in a 96 well plate).

3.2.3.3 Gene Expression in Static 3D Culture

Expression of BMP-2 on day 5, 7, and 10 was determined by real-time polymerase chain reaction (RT-PCR). The scaffolds were washed twice with phosphate buffered saline, removed from culture, homogenized in 1mL of Trizol (Invitrogen), and then stored at -70°C until further isolated. Then, the samples were transferred to a phase lock gel tube and incubated at room temperature for 5 minutes. Then the samples were vigorously agitated with 200 μL of chloroform for 15 seconds followed by incubation at room temperature for 3 minutes. The samples were centrifuged at 12000x g at 2 °C for 15 minutes to initiate the separation of the organic and aqueous phases. The aqueous phase, which contained the RNA, was placed in a new reaction tube and precipitated with equal volume of nuclease-free 70% ethanol. The precipitate were then processed using the RNeasy mini kit (Qiagen, Valencia, CA) according to the manufacturer's instructions, including the DNA digestion step with the DNAseI reagent (Qiagen). The mRNA was collected in 40 μL of RNAse-free water. Equal volumes (9 μL) of RNA were then reverse transcribed to cDNA using the Superscript First Strand kit (Invitrogen) with random hexamers as primers according to the manufacturer's instructions. RT-PCR then performed with the ABI 7300 Real Time PCR System (Applied Biosciences) and SYBR Green Master Mix (Applied Biosciences). The primers are shown in Table 3.1, with beta actin being the internal reference gene. The $2^{-\Delta\Delta Ct}$ method was used to quantify the gene expression [75].

Gene	Forward primer
Beta actin	5'-TGC TCC CCG GGC TGT ATT-3'
BMP-2	5'-CGC AGC TTC CAT CAG GAA -3'
	Reverse primer
Beta actin	5'-ACA TAG GAG TCC TTC TGA CCC ATT -3'
BMP-2	5'-CCC GGA AGA TCT GGA GTT CTG -3'

Table 3.1 PCR primers.

3.2.4 Static 2D Culture of MB-Luc and MC3T3-E1 Cells

To evaluate the luciferase activity and BMP-2 expression of both MB-Luc and MC3T3-E1 cells, the cells were cultured under static 2D conditions for up to 14 days. Cells were cultured in growth media and passaged before confluency. At day zero, the cells were seeded in 12 well plates at 1000 cells/mL and cultured in phenol red-free differentiation media. Assays were performed in duplicate at day 3, 5, 7, 9, 11, and 14.

3.2.4.1 Cell Number in 2D Culture

Cell number in 2D culture was determined at by PicoGreen® Assay (Invitrogen). Cell layers were scraped and collected in 500 µL of digestion buffer (100 mM NaCl, 10 mM Tris, 25 mM EDTA, 0.5% SDS, 0.1 mg/mL proteinase K (Fisher Scientific), pH 8) and stored at -70°C until analyzed. To quantify the DNA in the layers, 1 µL of the lysate was combined with 99 µL of TE buffer (10 mM Tris-HCl, 1 mM EDTA, pH 7.5) and 100 µL of PicoGreen® working reagent (1:200 dilution of dye to TE buffer). The sample fluorescence was measured with an excitation of 480 nm and an emission of 520 nm. DNA quantification was determined with a linear fit to a λ-bacteriophage DNA standard (0-1000 ng/mL). The total amount of DNA was determined by scaling up to the initial 500 µL of digestion buffer.

3.2.4.2 Luciferase Activity in 2D Culture

Luciferase activity was determined by luminometry. Cell layers were scraped and collected in 100 μL 1X Passive Lysis Buffer (Promega), and stored at -70°C until analyzed. Then, 20 μL of the lysate was combined with 100 μL of Luciferase Assay Substrate (Promega) and read in the LmaxII 384 Luminometer (Molecular Devices, Sunnyvale, CA), with a 10 s integration time. The luciferase activity was normalized by cell number.

3.2.4.3 Gene Expression in 2D Culture

BMP-2 expression in 2D culture was determined by RT-PCR. The cell layers were twice with PBS, scraped, and collected in 350 μL RLT buffer plus 3.5 μL of β-mercaptoethanol. The lysate was spun in a QIAShredder at 13300 rpm for 2 minutes. The flow through was then stored at -70°C for further isolation. The mRNA was from the lysate was isolated using the RNeasy mini kit (Qiagen), including the DNAseI digestion step, according to the manufacturer's instructions. The mRNA was collected in 40 μL of RNAse-free water. The total mRNA was quantified using the Quant-iT Ribogreen® RNA assay kit (Invitrogen). Next, 1 μg of RNA was reverse transcribed to cDNA using the Superscript First Strand kit (Invitrogen) with random hexamers as primers according to the manufacturer's instructions. RT-PCR then performed under the conditions listed in Section 3.2.3.3 and the primers previously listed in Table 3.1.

3.2.5 Perfusion Culture

MB-Luc cells were dynamically cultured under flow perfusion in chitosan using the flow system described in Section 2.2.1. MB-Luc cells were enzymatically lifted with 1X trypsin/EDTA and made into a suspension of 200,000 cells/mL using phenol red-free growth media. One mL of cell suspension was then injected into the center of the chitosan scaffold with an 18 gauge needle. The scaffold was incubated in with phenol red-free growth media overnight to allow for cell attachment. Next the scaffold was placed in the bioreactor in the perfusion flow loop with phenol red-free differentiation media plus 25mM HEPES buffer (Sigma). The tubing was pinched to maintain the flow rate of 3 mL/min (flow meter reading of 15).

For the first dynamic culture study, cells were cultured in the scaffold for six days, and upon completion of the culture, the scaffold was cut into three pieces for analysis of cell viability, gene expression, and luminometry. For the second dynamic culture study, cells were

culture in the scaffold for 11 days and analyzed by bioluminescence imaging each day starting at day 4.

3.2.5.1 Cell Viability in Perfusion Culture

To determine cell viability in the scaffold of the first dynamic culture, one piece was incubated in working MTT reagent as described in Section 3.2.3.1. After the four hour incubation, the scaffold was visibly observed for color change.

3.2.5.2 Luciferase Activity in Perfusion Culture

Luciferase activity was determined by luminometry. The piece of scaffold designated for luciferase activity determination was cut into two pieces, weighed wet, homogenized in 500 µL of 1X Passive Lysis Buffer (Promega), and stored at -70°C until analyzed. Then, 20 µL of the lysate was combined with 100 µL of Luciferase Assay Substrate (Promega) and read in the LMaxII 384 luminometer (Molecular Devices), with a 10 s integration time.

3.2.5.3 Gene Expression in Perfusion Culture

BMP-2 expression was determined by RT-PCR. The piece of scaffold designated for gene expression determination was cut into two, weighed wet, and homogenized as described in Section 3.2.3.3. RT-PCR was performed as described in Section 3.2.3.3 using the beta actin and BMP-2 primers listed in Table 3.1.

3.2.5.4 Bioluminescence Imaging of Perfusion Culture

Bioluminescence imaging was performed from day 4 to day 11 of perfusion culture. First, the excess volume of media contained within the reservoir was removed and 4-5 mL of working concentration of D-luciferin (100 µL of D-luciferin in 1 mL of phenol red-free media) was added to the flow system. The media was circulated through for 20 minutes, the flow was stopped, and the chamber was mounted in the imaging setup as previously described in Chapter 2. Imaging was performed with the PhotonMAX:512B camera (Princeton Instruments), with the following settings: 4 x 4 ROI binning, 100 second exposure time per face, controller gain 3, avalanche gain 4000, fast mode timing, ADC offset 270, and f/1.4.

3.3 Results/Discussion

3.3.1 Cell Viability and Alkaline Phosphatase Activity in Static 3D Culture

The ability of chitosan to serve as a suitable scaffold material for support of MC3T3-E1 cells was measured by the MTT and ALP assays. Chitosan has been widely studied as a supporting biomaterial for osteoblastic differentiation; however, we wanted to ensure that the fabrication techniques we were using in our laboratory for this material would support osteoblastic differentiation. Cell viability in static 3D culture was determined by the MTT assay as described in Section 3.2.3.1. The absorbance of the scaffolds as compared to blank is shown in Figure 3.1.

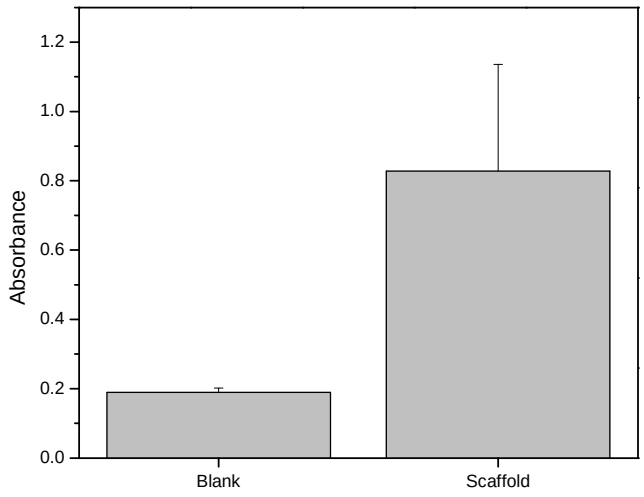

Figure 3.1 MTT results of MC3T3-E1 cells in static 3D culture. Data are shown as mean (n=3) plus standard deviation.

The results show an increase in optical density between the DMSO incubated with a blank well and the scaffolds. Alkaline phosphatase activity of the cells in the chitosan scaffolds was measured as described in Section 3.2.3.2. The alkaline phosphatase activity for the scaffolds on day 7 and 14 is shown in Figure 3.2.

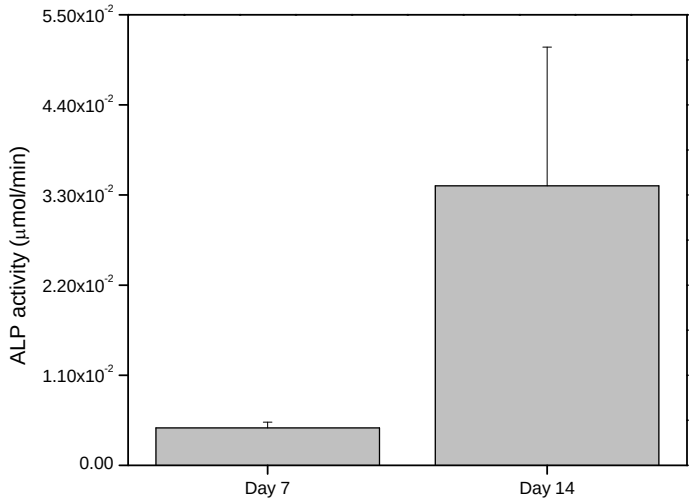

Figure 3.2 ALP activity of MC3T3-E1 cells in static 3D culture. Data are shown as mean (n=3) plus standard deviation.

The results for the MTT and ALP assays indicate that not only the cells were viable on the scaffold (indicated by MTT), but they were exhibiting elevated levels of ALP activity from day 7 to day 14 of culture. These results suggest that the MC3T3-E1 cells were undergoing osteoblastic differentiation in the chitosan scaffolds, and thus would be suitable for perfusion studies.

3.3.2. Gene Expression in Static 3D Culture

BMP-2 expression was determined in statically-cultured chitosan scaffolds. The goal was to characterize gene expression as a function of the supporting biomaterial to serve as a basis for gene expression in perfusion culture. Gene expression was analyzed on day 5, 7, and 10 of static culture as described in Section 3.2.3.3.

The beta actin Ct values ranged from 20.15-35.25, while the BMP-2 Ct values were mostly undetectable. The BMP-2 Ct values that were detectable ranged from 35.37-39. At first, we attempted to quantify the mRNA with the Ribogreen® assay at a 1:200 dilution. However, the mRNA from the scaffolds was undetectable at this dilution. So, to reverse transcribe the mRNA to cDNA, equal maximum volumes (9 µL) of the isolated mRNA were used to ensure

that sufficient cDNA would be produced. However, since the mRNA was not detected when quantified, the difficulty in detecting BMP-2 may be due to the low amount of mRNA isolated from the chitosan scaffolds. This result may be expected since chitosan is a positively charged material while RNA is negatively charged. Yet the beta actin Ct values do suggest that sufficient cDNA was present in the PCR reaction for amplification. This result may suggest that BMP-2 was not being produced in the static chitosan scaffolds. BMP-2 has been shown to be upregulated in perfusion culture, and may not have been produced in any detectable quantities in static culture [76].

3.3.3. Cell Number and Luminescence of Static 2D Culture

MB-Luc and MC3T3-E1 cells were statically cultured as described in Section 3.2.4, and analyzed for analyzed for cell number and luciferase activity. Figure 3.3 shows the number of cells in each cell type from days 3-14.

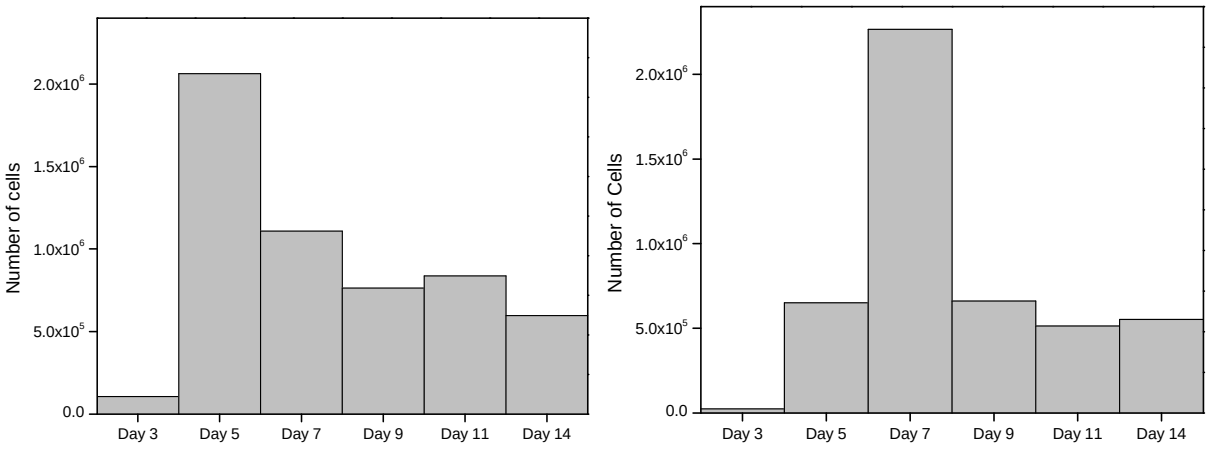

Figure 3.3 Cell number for MC3T3-E1 (left) and MB-Luc cells (right).

The cell numbers suggest that both cells types had a period of proliferation between day 3 and 7, beyond which the cell numbers leveled off. These results may indicate a termination of proliferation around day 7, and possibly some cell death beyond that time point. Cells layers were still viable in 2D culture beyond day 7.

Luciferase activity of the cells in 2D static culture was determined as described in Section 3.2.4.2. Figure 3.4 shows the luminescence intensity for the MB-Luc cells. The absolute

luminescence rose from day 3 to day 7, dropped at day 9 and peaked again at day 11. The low amount of collection buffer (100 μL) made collection of the cells difficult, and repeated 2D culture is required to confirm this result. The relative luminescence in the MC3T3-E1 cells at day 7 was 1.074×10^{-7} RLU/cell, indicating minimal luminescence when compared to the MB-Luc cells.

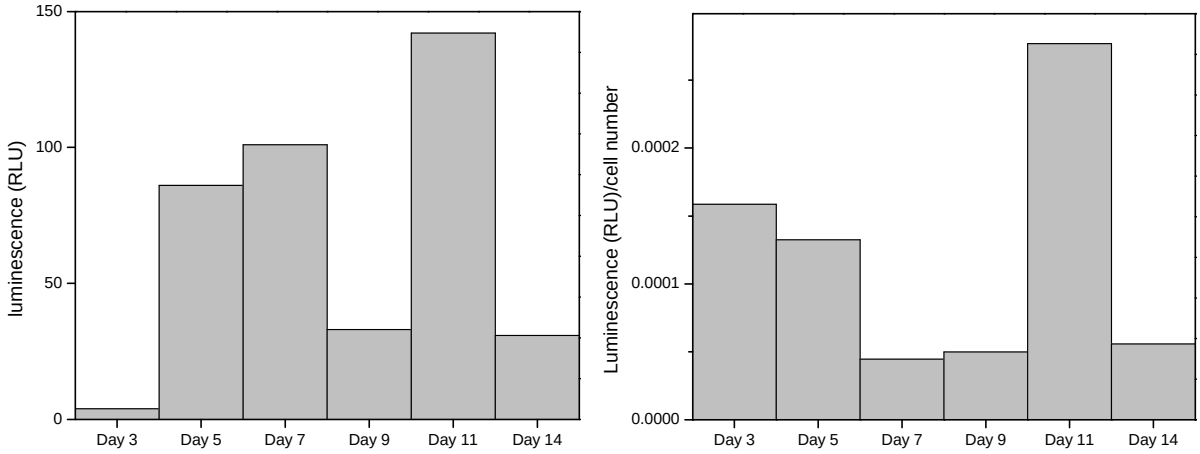

Figure 3.4 Luminescence (in relative light unit, left) and luminescence normalized per cell number for MB-Luc cells (right).

3.3.4. Gene Expression of Static 2D Culture

To determine the expression of BMP-2 in the static 2D culture, PCR was performed on each cell type as described in Section 3.2.4.3. The relative expression for MB-Luc and MC3T3-E1 cells is shown in Figure 3.5. The BMP-2 mRNA expression for both cell types appeared to peak around day 9, though this peak was not statistically significant.

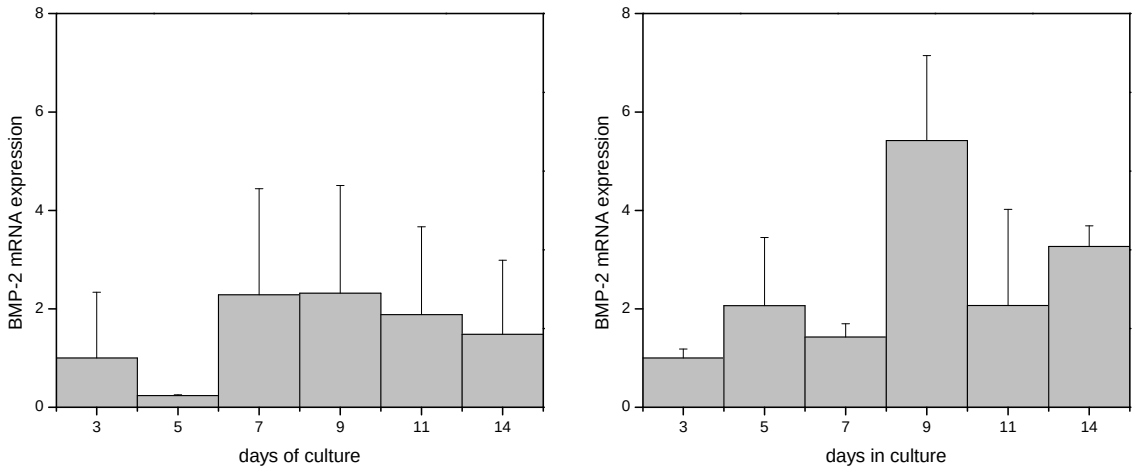

Figure 3.5 Relative mRNA expression of BMP-2 in MB-Luc (left) and MC3T3-E1 (right) cells. Data are shown with mean (n=2) and standard error.

3.3.5 Analysis of Perfusion Culture

MB-Luc cells were cultured under perfusion flow in chitosan as described in Section 3.2.5. The first study was run for six days, and following completion the scaffold was analyzed for cell viability, luciferase activity, and gene expression. To determine cell viability, a piece of the scaffold was incubated with the MTT reagent as previously described. Figure 3.6 shows the scaffold piece incubated with MTT.

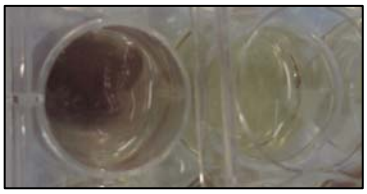

Figure 3.6 Scaffold incubated with MTT (left) and blank reagent (right).

The scaffold distinctly stained purple, as compared to the blank reagent. The purple also appeared to be evenly distributed throughout the scaffold, indicating that the cells were viable throughout the entire construct after six days of perfusion culture. Two pieces of scaffold from the first study were analyzed for luciferase activity by luminescence. The luminescence from these pieces was not detectable and instead similar to the luminescence of the MC3T3-E1 cells at

day 7. This result may be simply due to the low levels of luciferase protein at day 6, or due to the difficulty in isolating the protein from the chitosan. Two pieces of scaffold from the first study were analyzed for gene expression. The PCR Ct values for beta actin ranged from 35.24-36.83 and the Ct values for BMP-2 were undetectable. We believe this result may be due to the difficulty in isolating mRNA from chitosan and the relative early time point in the study.

Bioluminescence imaging was performed on the scaffold from the second perfusion study. The bioluminescence image for each face of the bioreactor from day 4 to day 11 is shown in Figure 3.7.

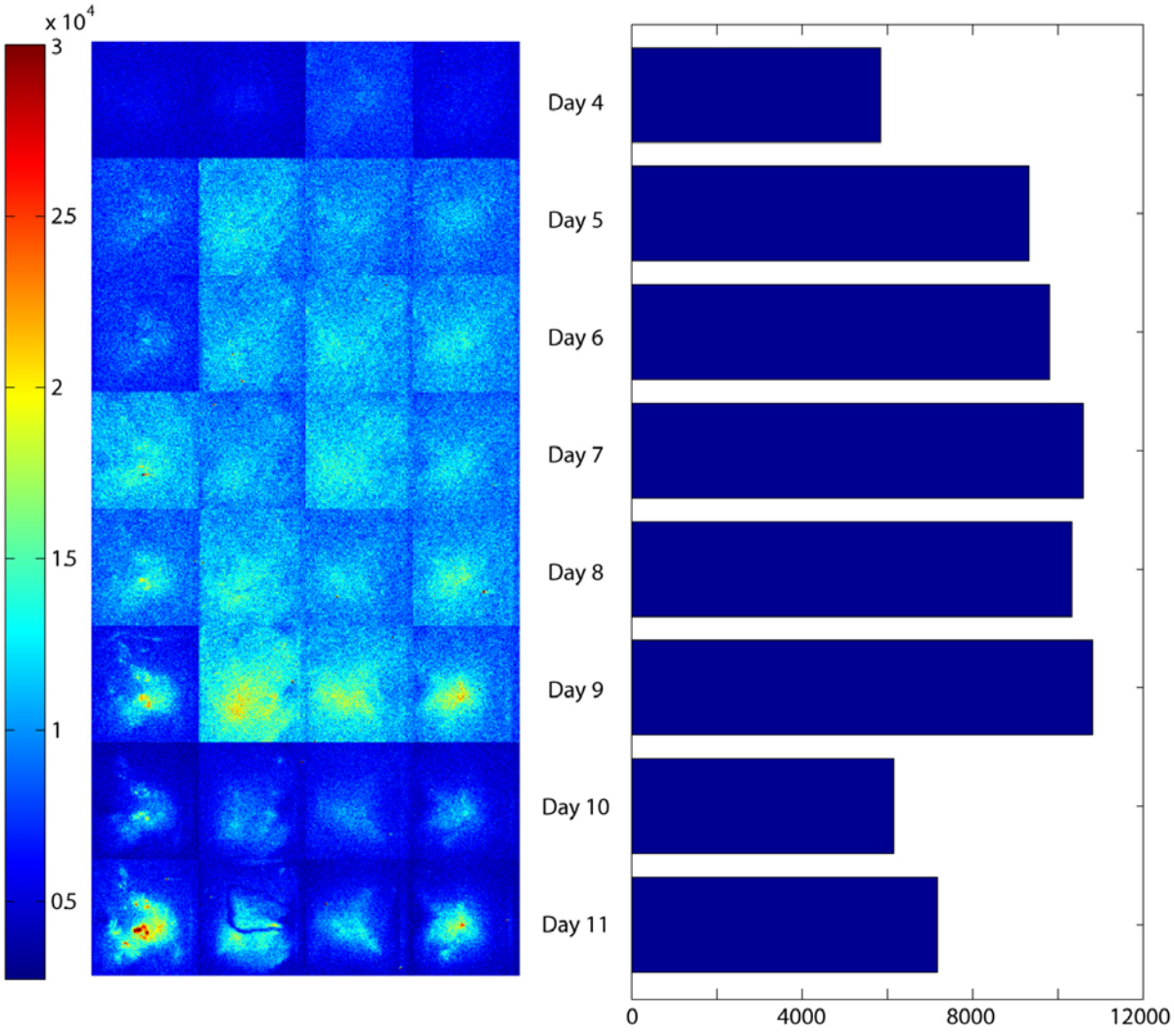

Figure 3.7 Bioluminescence images of MB-Luc cells undergoing flow perfusion (left), and average intensity per day (right, photons per pixel). Each row contains the four faces of the bioreactor.

Bioluminescence intensity increased from day 4 to day 7, and remained at a similar intensity until day 10, at which point the intensity markedly decreased. Two factors may be coming into play with this trend. First, the delivery method for the substrate may not be very efficient. Initially, the flow loop contained an injection point for the substrate immediately above the bioreactor. This design was intended to immediately deliver and distribute the substrate to the scaffold; however, with this method, it was difficult to actually inject the total volume of substrate into the entire chamber. Instead, excess media was removed from the reservoir and the working concentration of the substrate was injected into the reservoir. Then, the media was circulated throughout the entire flow loop. This process resulted in a significantly decreased working concentration of substrate that reached the scaffold, as well as a potentially large variation in the concentration of substrate from day to day.

Second, the background signal from each day and, in some cases, from face to face on the same day, varied. However, Figure 3.7 shows each face with the same background subtraction based on the background from day 4. This background subtraction may have contributed to an apparent decrease in signal at days 10 and 11. The specific 4 × 4 binning and gain settings may have contributed to this variation in background signal. Likely, the background for each face for each day must be determined to do a more exact comparison of the bioluminescence signal from day to day.

Third, it may be possible that the luciferase activity began to decrease in perfusion culture at day 10, though this result does not necessarily exactly correlate with the static culture data. Repeated studies, both in static and perfusion culture will be required to confirm such a result.

The bioluminescence signal appeared to be more intense in certain localized areas of the scaffold. For example, on day 11, the signal clearly originated around a kink in the scaffold (Figure 3.8).

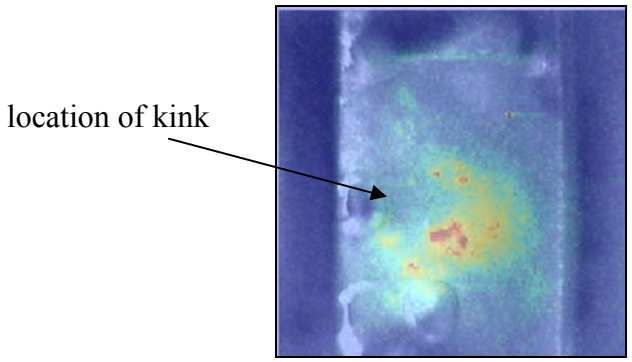

Figure 3.8 Combined brightfield and bioluminescence image of face 1 on day 11.

This result suggests that BMP-2 was not being produced throughout the entirety of the scaffold. Previous work done to localize BMP-2 in perfused scaffolds suggests that BMP-2 is highly localized to cells and the surrounding matrix [37]. To verify that BMP-2 is present in higher concentrations in certain areas of the scaffold, histological analysis and immunohistochemical staining of the scaffold will be required. Repeated flow perfusion studies will be required to determine if similar behavior continually occurs.

The bioluminescence intensity is very low in comparison to other *in vivo* models [54]. This result may be a consequence of the two previously mentioned limitations of the study. Additionally, the specific gain settings on the camera necessary to detect the bioluminescent photons were very high for this application, which may imply lower bioluminescence intensity than the images suggest. This result may suggest that the seeding density for the scaffolds (200,000 cells) is simply too low for this application. It may also suggest the BMP-2 expression is very low in this specific *in vitro* setting.

3.4 Conclusions

The overall goal of this study was to visualize the induction of BMP-2 in a perfused scaffold by bioluminescence imaging. First, the scaffold material chitosan was evaluated for use as a biomaterial for these specific experiments. Second, the MB-Luc cell line was tested to determine its effectiveness for the subsequent imaging of BMP-2 induction. Third, the cell-scaffold constructs were evaluated by bioluminescence imaging while undergoing flow perfusion. The images obtained from this study suggest that not only was BMP-2 being

produced in the scaffold, but that it was localized to distinct areas. Overall, these results indicate that this technology can provide useful information about BMP-2 expression in a perfused scaffold.

Chapter 4: Conclusions and Future Work

4.1 Conclusions

This research describes the design and construction of a 3D perfusion bioreactor suitable for cell culture and bioluminescence imaging. Chapter 2 describes the overall design of the system and describes the investigation into the feasibility of this system for bioluminescence imaging. The results indicate that bioluminescent cells can be detected by the system even at low cell numbers. This result applies to both transparent and translucent media, and to both cellular point sources and uniform cell distributions.

Chapter 3 describes the investigation of BMP-2 expression in a perfused cell-seeded scaffold by use of a bioluminescent reporter gene. Cells were transfected to express a BMP-2 luciferase reporter, seeded onto a scaffold, and imaged in the bioreactor after several days of perfusion flow. The results indicate that the BMP-2 luciferase was detectable by bioluminescence imaging and localized to certain areas of the scaffold. Further work is needed to confirm whether result is repeatable. Nevertheless, this strategy yielded information about the BMP-2 expression in a spatial and temporal manner that is not available with current assays.

4.2 Future Work

There are many variables, both directly related to these experiments and to the field overall, that can be addressed in future work.

4.2.1. Histological Analysis of Scaffolds

The majority of the *in vivo* bioluminescence imaging studies utilize histological analysis of the implant site to localize the cellular response in the scaffold. Due to the size of this bioreactor, histological analysis is an appropriate technique for localization of the cells. The scaffold would be cut to fit the embedding cassette, fixed in neutral buffered formalin, embedded in paraffin, and sectioned into 10 μm slices. These slices would be mounted onto glass slides for staining. The cells transfected with the pRL-SV40 vector would be stained with hemotoxylin and eosin, while cells transfected with the BMP-2-Luc vector can be immunostained for BMP-2. The hemotoxylin/eosin staining would provide direct evidence of cell location within a scaffold, and immunohistochemical staining for BMP-2 would provide direct evidence of BMP-2

expression within a scaffold. Ideally, it would be possible to see areas of the scaffold in which BMP-2 accumulation was higher, and correlate these areas to areas on higher bioluminescence.

4.2.2. Bioluminescence Tomography

Bioluminescence tomography is the quantitative localization and reconstruction of the bioluminescent signal. The bioreactor system provides a model optical environment for the application of bioluminescence tomography. The rectangular geometry is simpler than an animal model, and the optical coefficients could be applied uniformly throughout the construct. First the finite element model of the diffusion approximation to the radiative transport equation would be computed for multiple bioluminescent sources. Then, the error between the recorded images and computed images would be minimized by regularization techniques. These techniques could be used to reconstruct the cellular behavior in a more quantitative manner.

4.2.3 Late Osteoblastic Marker Reporters

Studies using transgenic mice with late osteoblastic markers in transgenic mice have been reported. In particular, osteocalcin [77] and bone sialo protein [78] have been investigated in this manner. For the applications described in this thesis, the MC3T3-E1 cells could be transfected with either promoter in the same manner as the BMP-2 promoter. The use of a late marker reporter would yield information about the late stages of osteoblastic differentiation in a cell-scaffold construct.

4.2.4 Dual Luciferase Labeling for Cell Viability and Gene Induction

Vilalta 2009 used dual reporter luciferase labeling to the monitor of cell viability and gene expression in an *in vivo* tissue engineering application [49]. They transfected CL1 cells with both a renilla luciferase reporter to monitor cell viability and a firefly luciferase to monitor the expression of type II procollagen. The cells were seeded onto demineralized bone matrix scaffolds and implanted into SCID mice. The authors then used the ratio of the renilla and firefly luciferases as a measure of chondrogenic differentiation.

A similar approach could be applied to this *in vitro* research. A slightly more complicated transfection procedure would be required to include a dual luciferase, and a band-pass filter would be required to detect the different wavelengths; however, the remainder of the

techniques could be applied in a similar fashion. The goal would be to localize cells expressing and not expressing BMP-2 within the scaffold.

4.3 Concluding Remarks

Overall, the applications of bioluminescence imaging to the tissue engineering field have not fully explored. However, this research addresses a major application of bioluminescence imaging by being the first to attempt image inside a bioreactor for the purpose of evaluating a cell-scaffold construct. The results obtained from this research indicate these strategies may yield useful information in addressing the development of a functional tissue replacement that may be applied to many areas of tissue engineering.

References

1. Giannoudis, P.V., H. Dinopoulos, and E. Tsiridis, *Bone subsitutes: An update.* Injury, 2005. **36S**: p. S20-S27.
2. Wheeler, D.L. and W.F. Ennekin, *Allograft Bone Decreases in Strength In Vivo over Time.* Clin. Orth. Rel. Res., 2005. **435**: p. 36-42.
3. Crane, G.M., S.L. Ishaug, and A.G. Mikos, *Bone tissue engineering.* Nature Med., 1995. **1**(12): p. 1322-1324.
4. Buckwalter, J.A., et al., *Bone Biology, Part 1: Blood Supply, Cells, Matrix, and Mineralization.* J. Bone Joint Surg., 1995. **77A**(8): p. 1256-1275.
5. Sikavitsas, V.I., J.S. Temenoff, and A.G. Mikos, *Biomaterials and bone mechanotransduction.* Biomaterials, 2001. **22**(19): p. 2581-2593.
6. Buckwalter, J.A., et al., *Bone Biology, Part 2: Formation, Form, Modeling, Remodeling, and Regulation of Cell Function.* J. Bone Joint Surg., 1995. **77A**(8): p. 1276-1289.
7. Lian, J.B. and G.S. Stein, *Concepts of Osteoblast Growth and Differentiation: Basis for Modulation of Bone Cell Development and Tissue Formation.* Crit. Rev. Oral. Biol. Med., 1992. **3**(3): p. 269-305.
8. Friedlaender, G.E., et al., *Osteogenic Protein-1 (Bone Morphogenetic Protein-7) in the Treatment of Tibial Nonunions.* J. Bone Joint Surg. Am., 2001. **83-A Suppl 1**(Pt 2): p. S151-S158.
9. Jones, A.L., et al., *Recombinant Human BMP-2 and Allograft Compared with Autogenous Bone Graft for Reconstruction of Diaphyseal Tibial Fractures with Cortical Defects. A Randomized, Controlled Trial.* J. Bone Joint Surg. Am., 2006. **88**(7): p. 1431-1441.
10. Saito, N., et al., *Local bone formation by injection of recombinant human bone morphogenetic protein-2 contained in polymer carriers.* Bone, 2003. **32**(4): p. 381-386.
11. Saito, N. and K. Takaoka, *New synthetic biodegradable polymers as BMP carriers for bone tissue engineering.* Biomaterials, 2003. **24**(13): p. 2287-2293.
12. Raiche, A.T. and D.A. Puleo, *In vitro effects of combined and sequential delivery of two bone growth factors.* Biomaterials, 2004. **25**(4): p. 677-685.
13. Uludag, H., et al., *Implantation of recombinant human bone morphogenetic proteins with biomaterial carriers: A correlation between protein pharmacokinetics and osteoinduction in the rat ectopic model.* J. Biomed. Mat. Res., 2000. **50**(2): p. 227-238.
14. Yamamoto, M., et al., *Bone regeneration by transforming growth factor [beta]1 released from a biodegradable hydrogel.* J. Controlled Release, 2000. **64**(1-3): p. 133-142.
15. Langer, R. and J.P. Vancanti, *Tissue Engineering.* Science, 1993. **260**(5110): p. 920-926.
16. Phillips, G.O., ed. *Bone Biology and Healing*. Allografts in Bone Healing: Biology and Clinical Applications. Vol. 1. 2003, World Scientific Publishing Pte Ltd: Singapore.
17. Greenwald, A.S., et al., *Bone-Graft Substitutes: Facts, Fictions, and Applications.* J. Bone Joint Surg. Am., 2001. **83**(2_suppl_2): p. S98-103.
18. Aubin, J.E., *Bone Stem Cells.* J. Cell. Biochem., 1998. **S30/31**: p. 73-82.
19. Franceschi, R.T. and B.S. Iyer, *Relationship Between Collagen Synthesis and Expression of Osteoblast Phenotype in MC3T3-E1 Cells.* J. Bone Mineral Res., 1992. **7**(2): p. 235-246.
20. Yang, S., et al., *The Design of Scaffolds for Use in Tissue Engineering. Part 1. Traditional Factors.* Tissue Eng., 2001. **7**(6): p. 679-689.

21. Ren, L., et al., *Novel approach to fabricate porous gelatin-siloxane hybrids for bone tissue engineering.* Biomaterials, 2002. **23**: p. 4765-4773.
22. Madihally, S.V. and H.W.T. Matthew, *Porous chitosan scaffolds for tissue engineering.* Biomaterials, 1999. **20**: p. 1133-1142.
23. Salgado, A.J., O.P. Coutinho, and R.L. Reis, *Bone Tissue Engineering: State of the Art and Future Trends.* Macromol. Biosci., 2004. **4**: p. 743-765.
24. Kim, I.-Y., et al., *Chitosan and its derivatives for tissue engineering applications.* Biotech. Adv., 2008. **26**: p. 1-21.
25. Jiankan, H., et al., *Fabrication and characterization of chitosan/gelatin porous scaffolds with predefinied internal microstructures.* Polymer, 2007. **48**: p. 4578-4588.
26. Gomes, M.E., et al., *Alternative tissue engineering scaffolds based on starch: processing methodologies, morphology, degradation and mechanical properties.* Mat. Sci. Eng. Part C, 2002. **20**: p. 19-26.
27. Hutmacher, D.W., *Scaffolds in tissue engineering bone and cartilage.* Biomaterials, 2000. **21**: p. 2529-2543.
28. Duarte, A.R.C., J.F. Mano, and R.L. Reis, *Preparation of chitosan scaffolds loaded with dexamethasone for tissue engineering applications using supercritical fluid technology.* European Polymer J., 2009. **45**: p. 141-148.
29. Liu, X., et al., *Pulsatile release of parathyroid hormone from an implantable delivery system.* Biomaterials, 2007. **28**(28): p. 4124-4131.
30. Portner, R., et al., *Bioreactor Design for Tissue Engineering.* Soc. Biotech. Japan, 2005. **100**(3): p. 235-245.
31. Martin, I., D. Wendt, and M. Heberer, *The role of bioreactors in tissue engineering.* Trends Biotech., 2004. **22**(2): p. 80-86.
32. Turner, C.H. and F.M. Pavalko, *Mechnotransduction and functional response of the skeleton to physical stress: The mechanisms and mechanics of bone adaptation.* J Orthopaedic Sci., 1998. **3**: p. 346-355.
33. Singer, V.L., et al., *Characterization of PicoGreen Reagent and Development of a Fluorescence-Based Solution Assay for Double-Stranded DNA Quantitation.* Anal. Biochem., 1997. **249**(2): p. 228-238.
34. Downs, T.R. and W.W. Wilfinger, *Fluorometric quantification of DNA in cells and tissue.* Anal. Biochem., 1983. **131**(2): p. 538-547.
35. Pauwels, R., et al., *Rapid and automated tetrazolium-based colorimetric assay for the detection of anti-HIV compounds.* J. Virological Meth., 1988. **20**(4): p. 309-321.
36. Cory, A.H., et al., *Use of an aqueous solulble tetrazolium/formazan assay for cell growth assays in culture.* Cancer Comm., 1991. **3**(7): p. 207-212.
37. Gomes, M.E., et al., *In Vitro Localization of Bone Growth Factors in Constructs of Biodegradable Scaffolds Seeded with Marrow Stromal Cells and Cultured in a Flow Perfusion Bioreactor.* Tissue Eng., 2006. **12**(3): p. 177-188.
38. van Lenthe, G.H., et al., *Nondestructive micro-computed tomography for biological imaging and quantification of scaffold-bone interactions in vivo.* Biomaterials, 2007. **28**: p. 2479-2490.
39. Porter, B.D., et al., *Noninvasive image analysis of 3D construct mineralization in a perfusion bioreactor.* Biomaterials, 2007. **28**: p. 2525-2533.
40. Rice, B.W., M.D. Cable, and M.B. Nelson, *In vivo imaging of light-emitting probes.* J. Biomed. Opt., 2001. **6**(4): p. 432-440.

41. de Wet, J.R., et al., *Firefly luciferase gene: structure and expression in mammalian cells.* Mol. Cell. Biol., 1987. **7**(2): p. 725-737.
42. Zhao, H., et al., *Emission spectra of bioluminescent reporters and interaction with mammalian tissue determin the sensitivity of detection in vivo.* J.Biomed. Opt., 2005. **10**(4): p. 0412101-9.
43. Hastings, J.W., *Chemistries and colors of bioluminescent reactions: a review.* Gene, 1996. **173**: p. 5-11.
44. Roda, A., et al., *Bioluminescence in analytical chemistry and in vivo imaging.* Trends Anal. Chem., 2009. **28**(3): p. 307-322.
45. Wood, K.W., et al., *Complementary DNA Coding Click Beetly Luciferases can Elicit Bioluminescence of Different Colors.* Science, 1989. **244**: p. 700-702.
46. Blum, J.S., et al., *Development and characterization of enhanced green fluorescent protein and luciferase expressing cell line for non-destructive evaluation of tissue engineering constructs.* Biomaterials, 2004. **25**(27): p. 5809-5819.
47. Román, I., et al., *Analysis of progenitor cell-scaffold combinations by in vivo non-invasive photonic imaging.* Biomaterials, 2007. **28**(17): p. 2718-2728.
48. Dégano, I.R., et al., *Bioluminescence imaging of calvarial bone repair using bone marrow and adipose tissue-derived mesenchymal stem cells.* Biomaterials, 2008. **29**(4): p. 427-437.
49. Vilalta, M., et al., *Dual luciferase labelling for non-invasive bioluminescence imaging of mesenchymal stromal cell chondrogenic differentiation in demineralized bone matrix scaffolds.* Biomaterials, 2009. **30**(28): p. 4986-4995.
50. Lui, J., et al., *In vitro and in vivo bioluminsecent imaging of hypoxia in tissue engineering grafts.* Tissue Eng. Part C Meth., 2009.
51. Han, W.M., W.X. Cong, and G. Wang, *Mathematical theory and numerical analysis of bioluminescence tomography.* Inv. Prob., 2006. **22**: p. 1659-1675.
52. Ntziachristos, V., et al., *Looking and listening to light: the evolution of whole-body photonic imaging.* Nature Biotech., 2005. **23**: p. 313-320.
53. Cong, W.X., et al., *A practical reconstruction method for bioluminescence tomography.* Opt. Exp., 2005. **13**: p. 6756-6771.
54. Wang, G., et al., *In vivo mouse studies with bioluminescence tomography.* Opt. Exp., 2006. **14**: p. 7801-7809.
55. Zalaba, M., et al., *Evaluation of bioluminescent imaging for noninvasive monitoring of colorectal cancer progression in the live and its response to immunogene therapy.* Mol. Cancer, 2009. **8**(2): p. *open access*.
56. Deroose, C.M., et al., *Metastatic Model Multimodality Imaging.* J. Nuc. Med., 2007. **48**: p. 295-303.
57. Dai, T., et al., *Chitosan Acetate Bandage as Topical Antimicrobial Dressing for Infected Burns.* Antimicrobial Agents and Chemotherapy, 2009. **53**(2): p. 393-400.
58. Engelsman, A.F., et al., *Real Time Noninvasive Montioring of Contaminating Bacteria in a Soft Tissue Implant Infection Model.* J. Biomed. Mat. Res. Part B: App. Biomat., 2009. **88**: p. 123-129.
59. Dunn, C.A., et al., *BMP Gene Delivery for Alveolar Bone Engineering at Dental Implant Defects.* Mol. Ther., 2005. **11**(2): p. 294-299.

60. Jang, J.-H., C.B. Rives, and L.D. Shea, *Plasmid Delivery in Vivo from Porous Tissue-Engineering Scaffolds: Transgene Expression and Cellular Transfection.* Mol. Ther., 2005. **12**(3): p. 475-483.
61. Dégano, I.R., et al., *The effect of self-assembling peptide nanofiber scaffolds on mouse embryonic fibroblast implantation and proliferation.* Biomaterials, 2009. **30**(6): p. 1156-1165.
62. Contag, C.H. and M.H. Bachmann, *Advances in in vivo bioluminescence imaging of gene expression.* Ann. Rev. Biomed. Eng., 2002. **4**: p. 235-259.
63. Kreke, M.R. and A.S. Goldstein, *Hydrodynamic Shear Stimulates Osteocalcin Expression but not Proliferation of Bone Marrow Stromal Cells.* Tissue Eng., 2004. **10**: p. 780-788.
64. Goldstein, A.S., et al., *Effect of convection on osteoblastic cell growth and function in biodegradable polymer foam scaffolds.* Biomaterials, 2001. **22**(11): p. 1279-1288.
65. Bancroft, G.N., V.I. Sikavitsas, and A.G. Mikos, *Design of a Flow Perfusion Bioreactor System for Bone Tissue-Engineering Applications.* Tissue Eng., 2004. **9**(3): p. 549-554.
66. Prahl, S.A., M.J.C. van Gemert, and A.J. Welch, *Determining the optical properties of turbid media by using the adding-doubling method.* App. Opt., 1993. **32**: p. 559-568.
67. Welch, A.J. and M.J.C. van Gemert, *Optical and Thermal response of laser-irradiated tissue*. 1995, New York: Plenum Press.
68. Zhao, H., et al., *Emission spectra of bioluminescent reporters and interaction with mammalian tissue determine sensitivity of detection in vivo.* J. Biomed. Opt., 2005. **10**(4): p. 0412101-9.
69. Carofino, B.C. and J.R. Lieberman, *Gene Therapy Applications for Fracture Healing.* J Bone Joint Surg., 2008. **90**(Suppl 1): p. 99-110.
70. Suphasiriroj, W., et al., *The fundamental parameters of chitosan in polymer scaffolds affecting osteoblasts (MC3T3-E1).* J. Mat. Sci. Mat. Med., 2009. **20**: p. 309-320.
71. Thein-Han, W.W. and R.D.K. Misra, *Biomimetic chitosan-nanohydroxyapatite composite scaffolds for bone tissue engineering.* Acta Biomat., 2009. **5**(4): p. 1182-1197.
72. Kong, L., et al., *A study on the bioactivity of chitosan/nano-hydroxyapatite composite scaffolds for bone tissue engineering.* European Polymer J., 2006. **42**(12): p. 3171-3179.
73. Arpornmaeklong, P., et al., *Growth and differentiation of mouse osteoblasts on chitosan-collagen sponges.* Int. J. Oral Maxillofacial Surg., 2007. **36**: p. 328-337.
74. Sharp, L.A., *The Use of Dynamic Fluid Flow Strategies for Bone Tissue Engineering Applications, PhD Dissertation*, in *Chemical Engineering*. 2009, Virginia Polytechnic Insitute and State University: Blacksburg, VA. p. 110.
75. Livak, K.J. and T.D. Schmittgen, *Analysis of Relative Gene Expression Data Using Real-Time Quantitative PCR and the 2-[Delta][Delta]CT Method.* Meth., 2001. **25**(4): p. 402-408.
76. Sharp, L., Y. Lee, and A. Goldstein, *Effect of Low-Frequency Pulsatile Flow on Expression of Osteoblastic Genes by Bone Marrow Stromal Cells.* Ann. Biomed. Eng., 2009. **37**(3): p. 445-453.
77. Bar, I., et al., *Molecular Imaging of the Skeleton: Quantitative Real-Time Bioluminescence Monitoring Gene Expression in Bone Repair and Developemt.* J. Bone Mineral Res., 2003. **18**(3): p. 570-578.
78. Chen, J., et al., *Altered Expression of Bone Sialoproteins in Vitamin D-Deficient rBSP2.7Luc Transgenic Mice.* J Bone Mineral Res., 1999. **14**(2): p. 221-229.

Appendix A. Finite Element Modeling of the Diffusion Approximation to the Radiative Transport Equation

A.1 Galkerin Projection

The Galkerin projection for the steady-state diffusion approximation to the radiative transport equation is achieved by multiplying the original equation by the interpolation function, ψ, and integrating the over the domain, Ω.

$$\int_\Omega \psi(\vec{x})\left[D\nabla^2\Phi(\vec{x}) - \mu_a\Phi(\vec{x})\right]d\Omega = -\int_\Omega \psi(\vec{x})S(\vec{x})\,d\Omega \tag{A.1}$$

Expanding the right hand side of the equation, and then using the chain rule to expand the first term:

$$\int_\Omega \psi(\vec{x})D\nabla^2\Phi(\vec{x})\,d\Omega - \int_\Omega \psi(\vec{x})\mu_a\Phi(\vec{x})\,d\Omega \tag{A.2}$$

$$\int_\Omega \psi(\vec{x})D\nabla^2\Phi(\vec{x})\,d\Omega = D\left[\int_\Omega \nabla\left(\psi\nabla\Phi\right)d\Omega - \int_\Omega \nabla\psi\cdot\nabla\Phi\,d\Omega\right] \tag{A.3}$$

The first integral on the right hand side can be converted from an integral over the domain Ω to an integral over the surface ∂Ω using the divergence theorem:

$$\int_\Omega \nabla\left(\psi\nabla\Phi\right)d\Omega = \oint_{\partial\Omega}\psi\nabla\Phi\cdot n\,dS \tag{A.4}$$

The Galerkin projection becomes:

$$D\oint_{\partial\Omega}\psi\nabla\Phi\cdot n\,dS - D\int_\Omega \nabla\psi\cdot\nabla\Phi\,d\Omega - \int_\Omega \psi\mu_a\Phi\,d\Omega = -\int_\Omega \psi S\,d\Omega \tag{A.5}$$

The surface integral is then defined in terms of Γ, or the exitance on the domain surface.[1,2] The final equation for the Galerkin projection becomes:

$$-D\int_\Omega \nabla\psi\cdot\nabla\Phi\,d\Omega - \int_\Omega \psi\mu_a\Phi\,d\Omega = \int_\Omega \psi S\,d\Omega + \int_{\partial\Omega}\Gamma\psi\,d(\partial\Omega) \tag{A.6}$$

The linear matrix system is constructed where the individual components of the matrices are defined,

$$\left([K]+[C]\right)(\Phi) = [S]+\beta \tag{A.7}$$

$$\begin{cases} K_{ij} = \int_{\Omega} D(\nabla \psi_i(\vec{x})) \cdot (\nabla \psi_j(\vec{x}))\, d\Omega \\ C_{ij} = \int_{\Omega} \mu_a \psi_i(\vec{x}) \psi_j(\vec{x})\, d\Omega \\ S_j = \int_{\Omega} S(\vec{x}) \psi_j\, d\Omega \\ \beta_j = \int \psi_j(\vec{x}) \Gamma(\vec{x})\, d(\partial\Omega) \end{cases} \tag{A.8}$$

while the photon density is discretized.

$$\Phi(\vec{x}) = \sum_{k=1}^{D} \Phi_i(\vec{x}) \psi_i \tag{A.9}$$

A.2 Domain Discretization

The volume of the bioreactor is discretized into 4 node-tetrahedron elements using a discretization level of 3. Each local element, X^E, contains the four nodes constructing the tetrahedral element.

$$X_i^E = \left(x_i^E, y_i^E, z_i^E\right) \tag{A.10}$$

To connect each local element to the global element array, each element is mapped to the parametric coordinate system so that:

$$X = X_1^E \psi_1(\xi,\eta,\gamma) + X_2^E \psi_2(\xi,\eta,\gamma) + X_3^E \psi_3(\xi,\eta,\gamma) + X_4^E \psi_4(\xi,\eta,\gamma) \tag{A.11}$$

where the interpolation function is chosen as the Kronecker delta between the i^{th} interpolation function and j^{th} node.

$$\psi_i\left(\xi_j, \eta_j, \gamma_j\right) = \delta_{ij} \tag{A.12}$$

The subsequent equations for the interpolation functions with the tetrahedral element whose 1^{st} node is located at the parametric origin are:

$$\begin{aligned} \psi_1 &= 1 - \xi - \eta - \gamma \\ \psi_2 &= \xi \\ \psi_3 &= \eta \\ \psi_4 &= \gamma \end{aligned} \tag{A.13}$$

Substituting in the interpolation functions into the mapping equations:

$$x = x_1^E + \left(x_2^E - x_1^E\right)\xi + \left(x_3^E - x_1^E\right)\eta + \left(x_4^E - x_1^E\right) \tag{A.14}$$

$$y = y_1^E + \left(y_2^E - y_1^E\right)\xi + \left(y_3^E - y_1^E\right)\eta + \left(y_4^E - y_1^E\right)\gamma \tag{A.15}$$

$$z = z_1^E + \left(z_2^E - z_1^E\right)\xi + \left(z_3^E - z_1^E\right)\eta + \left(z_4^E - z_1^E\right)\gamma \tag{A.16}$$

To transform any function, f(x,y,z), into parametric coordinates:

$$\iiint f(x,y,z)dxdydz = \iiint f(\xi,\eta,\gamma)h_v d\xi d\eta d\gamma \tag{A.17}$$

where h_v volume metric coefficient, and is six times the volume of tetrahedral element. It is calculated from the determinant of the matrix J:

$$h_v \equiv Det(J) = \left(\frac{\partial X}{\partial \xi} \times \frac{\partial X}{\partial \eta}\right) \cdot \frac{\partial X}{\partial \gamma} = 6V \tag{A.18}$$

$$J = \begin{bmatrix} \frac{\partial x}{\partial \xi} & \frac{\partial x}{\partial \eta} & \frac{\partial x}{\partial \gamma} \\ \frac{\partial y}{\partial \xi} & \frac{\partial y}{\partial \eta} & \frac{\partial y}{\partial \gamma} \\ \frac{\partial z}{\partial \xi} & \frac{\partial z}{\partial \eta} & \frac{\partial z}{\partial \gamma} \end{bmatrix} = \begin{bmatrix} x_2^E - x_1^E & x_3^E - x_1^E & x_4^E - x_1^E \\ y_2^E - y_1^E & y_3^E - y_1^E & y_4^E - y_1^E \\ z_2^E - z_1^E & z_3^E - z_1^E & z_4^E - z_1^E \end{bmatrix} \tag{A.19}$$

The matrices necessary for the finite element construction are the element diffusion matrix, A, and the element mass matrix, B.

$$A_{ij}^l = \iiint_{El} \nabla\psi_i \nabla\psi_j dxdydz = 6V \iiint_{El} \nabla\psi_i \nabla\psi_j d\xi d\eta d\gamma \tag{A.20}$$

$$B_{ij}^l = \iiint_{El} \psi_i \psi_j dxdydz = 6V \iiint_{El} \psi_i \psi_j d\xi d\eta d\gamma \tag{A.21}$$

These matrices can be substituted into the linear system.

$$K_{ij} = DA_{ij} \tag{A.22}$$

$$C_{ij} = \mu_a B_{ij} \tag{A.23}$$

A.3 Boundary Conditions

For these experiments, the data are collected in a dark room. Thus, there are effectively no external photons introduced to the system, so that:

$$\Phi(x) = 0 \quad for\ x \notin \Omega \tag{A.24}$$

The simplest boundary condition to apply to this system is the Dirichlet boundary condition, in which there is no photon density on the boundary of the system.

$$\Phi(x) = 0 \quad for\ x \in \partial\Omega \tag{A.25}$$

Physically, this condition is not very accurate, as it effectively means the surrounding medium is a perfect absorber of photons that exit the domain.[2,3] The more physically relevant boundary condition is the Robin boundary condition, in which the photon propagation from the domain to the external medium is governed by the change in the index of refraction from the domain to the external medium:

$$\Phi(\vec{x}) + 2DA'\hat{n}\cdot\nabla\Phi(\vec{x}) = 0 \tag{A.26}$$

Where $\hat{n}$ is the unit normal to $\partial\Omega$ at x, A' is the parameter that accounts for the index mismatch and n is the index of refraction within Ω, assuming n' for the surrounding medium is equal to 1:

$$A' = \frac{(1+R)}{(1-R)}, \quad R \approx -1.4399n^{-2} + .7099n^{-1} + .0636n + .6681 \tag{A.27}$$

For n=1.37 (approximate for biologics), A' is equal to .1639. To implement the Robin boundary condition, the normal derivative is written as, and rearranged and written with a surface integral.

$$\frac{\partial\Phi(x)}{\partial n} = f(x)\Phi(x) + g(x) \tag{A.28}$$

$$\int_{\partial\Omega}\psi(x)\Gamma(x)d(\partial\Omega) = -\int\psi(x)cD[f(x)\Phi(x) + g(x)]d(\partial\Omega) \tag{A.29}$$

Substituting for f(x) and g(x):

$$\left.\begin{aligned} f(x) &= -\frac{1}{2DA'} \\ g(x) &= 0 \end{aligned}\right\} \tag{A.30}$$

The overall matrix equation can be rearranged to include matrix F.

$$([K]+[C]+[F])(\Phi) = [S] \tag{A.31}$$

$$F_{ij} = \frac{c}{2A'}\int_{\partial\Omega}\psi_j(x)\psi_i(x)d(\partial\Omega) \tag{A.32}$$

A.4 Source Conditions

For bioluminescent reconstruction, the actual source is determined by minimization of error between the scattering behavior from a predetermined source and the actual scattering behavior measured by experiment. Thus, the source for the forward problem can be selected in the manner in our choosing. The source approximations can be divided into two different categories: a collimated source, in which the source is defined as an isotropic point, or a diffuse source in which a separate domain, Ω_2, is defined as the source and entirely contained within Ω.[2]

The collimated source is easiest to implement:

$$S_i = q_s(r_s)\psi_i(r_s) \tag{A.32}$$

where q_s is the strength of the photon source at r_s. The diffuse point source is slightly more complicated to implement. For a diffuse source with strength Γ_s contained within Ω_2, the source term is defined below.

$$S_i = \frac{2\Gamma_s}{A'}\psi_i(\xi_s), \quad \xi_s \in \Omega_2 \tag{A.33}$$

A.5 References

1. Cong, W.X., et al., *A practical reconstruction method for bioluminescence tomography.* Opt. Exp., 2005. **13**: p. 6756-6771.
2. Schweiger, M., et al., *The finite element method for the propagation of light in scattering media: boundary and source conditions.* Med. Phys., 1995. **22**(11): p. 1779-1792.
3. Arridge, S.R., et al., *A finite element approach for modeling photon transport in tissue.* Med. Phys., 1993. **20**(2): p. 299-309.

Appendix B. Representative Code for Image Processing

B.1 Speread

All of the images collected with either the VersArray camera or Photon Max camera were saved in .spe format. The .spe format is generally associated with Princeton Instruments equipment and WinView 32 Software. The .spe files are imported into Matlab using a function called speread. Speread was written by Dr. Haiou Shen at Virginia Tech.

```
function [X, xdim, ydim, exptime, numframe] = speread(filename)
% read 16-bits spe image file for format v2.5.
% by Haiou Shen
fid = fopen(filename);
fseek(fid,10,'bof');
exptime = fread(fid,1,'float');
fseek(fid,42,'bof');
xdim    = fread(fid,1,'uint16');
fseek(fid,656,'bof');
ydim    = fread(fid,1,'uint16');
fseek(fid,1446,'bof');
numframe = fread(fid,1,'uint32');
fseek(fid,4100,'bof');
X=uint16(zeros(ydim, xdim, numframe));
for K=1:numframe
    for I = 1:ydim,
        X(I,:,K)=fread(fid,xdim,'uint16');
    end
end
fclose(fid);
```

B.2 Image Processing

In chapter 2, the four faces were displayed in one image. To accomplish this, the images were first imported with speread:

```
[Img1, xdim, ydim, exptime, numframe] = speread('face1.SPE');
[Img2, xdim, ydim, exptime, numframe] = speread('face2.SPE');
[Img3, xdim, ydim, exptime, numframe] = speread('face3.SPE');
[Img4, xdim, ydim, exptime, numframe] = speread('face4.SPE');
```

Next, the background signal was subtracted from each image. The background was about 155 photons per pixel using the VersArray camera.

```
Img1=Img1-155;
Img2=Img2-155;
Img3=Img3-155;
Img4=Img4-155;
```

The images were combined into one image.

```
NewImg = [Img1, Img2; Img3, Img4];
```

The new image can be displayed with the command imshow.

```
imshow(NewImg, [0, max(max(NewImg))]);
colorbar;
```

The scale can be adjusted by changing the upper limit from max(max(NewImg)) to a lower number.

```
imshow(NewImg, [0, 1500]);
colorbar;
```

The images are automatically displayed in grayscale. For the work in this thesis, the "jet" colormap was applied.

Appendix C. Inverse Adding-Doubling Data File for Porous Chitosan

C.1 Inverse Adding-Doubling Data File

The optical coefficients of porous chitosan were determined by the inverse adding-doubling method. The program used was developed by Dr. Scott Prahl at the Oregon Health and Science University. It is available for download at http://omlc.ogi.edu/software/iad/. The data file, which contains the spectral information for porous chitosan based on my measurements, is listed here. The data file is then run in the executable program to calculate the optical coefficients.

```
IAD1

1.52 # Index of refraction
1.50 # Index of refraction of top and bottom slides
.6   # Thickness of sample
1.00 # Thickness of slides
2.00 # Diameter of illumination beam
1.00 # Reflectivity of the reflectance calibration standard

0 # Number of spheres used in the measurement

150.0
25.4
12.7
1.00
.96

150.0
25.4
12.7
1.00
.96

2 # Number of measurements, M_R, M_T

#lambda      M_R           M_T
1300    0.171135559    0.597476082
1299    0.171739559    0.598408508
1298    0.171201897    0.598877411
1297    0.172118645    0.599583321
1296    0.172371006    0.600772018
1295    0.172147636    0.600868568
1294    0.172893009    0.601556168
1293    0.173021298    0.602168808
1292    0.17283144     0.602701531
1291    0.173090553    0.603055077
1290    0.173458958    0.604018707
1289    0.173857021    0.604729996
1288    0.173658218    0.605000305
1287    0.174092636    0.605529976
1286    0.174279995    0.60585125
1285    0.17424921     0.606054726
1284    0.174381199    0.606737862
1283    0.174305954    0.60682045
1282    0.174948311    0.607096138
1281    0.174827328    0.60707901
1280    0.175096531    0.607462997
1279    0.175195923    0.607491379
1278    0.174928093    0.608137856
1277    0.175368805    0.608035164
1276    0.174546547    0.608859787
1275    0.175364494    0.608636971
1274    0.175308323    0.608678169
```

1273	0.175224457	0.609189529
1272	0.175502186	0.60905098
1271	0.175688896	0.609015694
1270	0.17523262	0.609355202
1269	0.175120926	0.608888817
1268	0.175307388	0.609341621
1267	0.175319576	0.60925293
1266	0.175256214	0.608996315
1265	0.175315647	0.6090588
1264	0.175189762	0.608747139
1263	0.175391274	0.608955154
1262	0.175230465	0.608768768
1261	0.175338688	0.608437195
1260	0.174954205	0.608267441
1259	0.175044498	0.608616409
1258	0.174984646	0.608023453
1257	0.174955368	0.608171692
1256	0.174893475	0.607405014
1255	0.174335918	0.607610626
1254	0.174880066	0.606919479
1253	0.174545803	0.606817436
1252	0.174854889	0.60656971
1251	0.174914055	0.606656609
1250	0.174577522	0.60607605
1249	0.174229584	0.606105804
1248	0.174209366	0.605969124
1247	0.173873406	0.605365295
1246	0.173977604	0.605418625
1245	0.174044094	0.604999733
1244	0.173470745	0.604691849
1243	0.173700466	0.604528656
1242	0.173658695	0.603550568
1241	0.173512306	0.603994789
1240	0.173535328	0.603218308
1239	0.173300552	0.603265038
1238	0.173272781	0.603226433
1237	0.17319355	0.602703438
1236	0.172913227	0.602343559
1235	0.172897816	0.601999092
1234	0.172844791	0.601557388
1233	0.172640839	0.60168457
1232	0.172947159	0.601855698
1231	0.17256794	0.601278763
1230	0.172569771	0.600686302
1229	0.17255085	0.601297188
1228	0.172624664	0.600656052
1227	0.17281086	0.600464172
1226	0.172461681	0.600476456
1225	0.172612495	0.600226746
1224	0.1724123	0.599571457
1223	0.172553577	0.599459953
1222	0.172189064	0.599859009
1221	0.172265377	0.599666061
1220	0.172558899	0.599151726
1219	0.172419033	0.59936821
1218	0.172417469	0.599160805
1217	0.17183054	0.598728523
1216	0.172394924	0.59856369
1215	0.171824551	0.59840023
1214	0.172111378	0.59779213
1213	0.171881924	0.598187447
1212	0.17185812	0.597497482
1211	0.171458607	0.597789688
1210	0.171743832	0.59765213
1209	0.171992073	0.597290459
1208	0.17168314	0.597103233
1207	0.171950035	0.597329216
1206	0.17192564	0.596819954
1205	0.171869049	0.596794052
1204	0.171806259	0.596543007
1203	0.172152329	0.596547241

1202	0.171828632	0.596616402
1201	0.171992569	0.596695824
1200	0.171661243	0.596252213
1199	0.172338982	0.598568802
1198	0.172624397	0.598195839
1197	0.172532883	0.598457031
1196	0.172869587	0.598225365
1195	0.172458839	0.597956772
1194	0.17277565	0.598013268
1193	0.172802219	0.598090172
1192	0.172713966	0.598744888
1191	0.172716446	0.598475761
1190	0.172870808	0.598456993
1189	0.173197575	0.598756485
1188	0.173087387	0.598733368
1187	0.173480759	0.598641701
1186	0.173376465	0.599149361
1185	0.173636723	0.599669762
1184	0.173645096	0.599799347
1183	0.173769054	0.599775734
1182	0.173693008	0.600078926
1181	0.173773937	0.600173225
1180	0.173830109	0.600652504
1179	0.173631592	0.600939102
1178	0.174110184	0.600655251
1177	0.174395599	0.600991592
1176	0.17421751	0.601143761
1175	0.174223862	0.601536331
1174	0.174540672	0.601183472
1173	0.174371758	0.60189743
1172	0.174670544	0.60199173
1171	0.174561501	0.602226677
1170	0.174987698	0.602371292
1169	0.174836655	0.602751122
1168	0.175275765	0.602860947
1167	0.17526535	0.603259583
1166	0.175913029	0.603119736
1165	0.175196819	0.603036881
1164	0.175437603	0.603684502
1163	0.175905743	0.604223442
1162	0.176080933	0.604791832
1161	0.176143761	0.605485687
1160	0.176478539	0.605705566
1159	0.176745853	0.606101532
1158	0.176664352	0.606648254
1157	0.177440472	0.606913452
1156	0.178056889	0.608773766
1155	0.178540726	0.609549866
1154	0.178642654	0.61090744
1153	0.179160118	0.611659889
1152	0.179553433	0.613401108
1151	0.180212116	0.615032387
1150	0.181187496	0.616149445
1149	0.181664372	0.617705765
1148	0.182184944	0.619915619
1147	0.18311121	0.622527351
1146	0.183888569	0.624207268
1145	0.184917755	0.625934258
1144	0.185543919	0.628325119
1143	0.186515465	0.631187248
1142	0.187321644	0.632361107
1141	0.188022976	0.635415306
1140	0.189041042	0.637211494
1139	0.189943047	0.639226265
1138	0.190320702	0.641808472
1137	0.191007824	0.643146668
1136	0.191740151	0.645070648
1135	0.192718563	0.647271195
1134	0.193171749	0.648365326
1133	0.193631401	0.649571381
1132	0.194249458	0.651053772

1131	0.195033398	0.65192688
1130	0.195544167	0.653012695
1129	0.195805512	0.654121552
1128	0.195800705	0.654582977
1127	0.196402321	0.655770187
1126	0.196419163	0.656141968
1125	0.196297131	0.656429215
1124	0.196844692	0.657383957
1123	0.197103863	0.657763443
1122	0.197092552	0.658327484
1121	0.197415066	0.658086777
1120	0.197577	0.658377686
1119	0.197219982	0.658794632
1118	0.197792397	0.658832092
1117	0.198016949	0.659619598
1116	0.198208542	0.659246368
1115	0.198088398	0.659753647
1114	0.198442974	0.659775467
1113	0.198047676	0.660296631
1112	0.198217163	0.660655747
1111	0.198539124	0.660212097
1110	0.198622761	0.660554886
1109	0.198460808	0.660576172
1108	0.198988895	0.661148224
1107	0.199005451	0.660648804
1106	0.199058285	0.660934067
1105	0.199183312	0.66091156
1104	0.198811989	0.661497955
1103	0.199423962	0.661958923
1102	0.19917057	0.66199585
1101	0.19960741	0.66211647
1100	0.199505043	0.662308502
1099	0.199266014	0.662107468
1098	0.199182549	0.6629776
1097	0.199602356	0.662472687
1096	0.199719467	0.662561874
1095	0.200089397	0.662708435
1094	0.199877567	0.662798233
1093	0.19990345	0.663167343
1092	0.200314903	0.66334404
1091	0.200128365	0.663470688
1090	0.200260944	0.66352684
1089	0.200516052	0.663637238
1088	0.200519295	0.663261261
1087	0.200476399	0.664056397
1086	0.200665779	0.664090118
1085	0.200892162	0.663398514
1084	0.200625114	0.663961945
1083	0.200762577	0.664233322
1082	0.200971031	0.664143295
1081	0.200856743	0.664546433
1080	0.200947723	0.664300079
1079	0.200264854	0.664331818
1078	0.200754395	0.664727631
1077	0.20120676	0.664423904
1076	0.201034699	0.664386597
1075	0.200793476	0.664277878
1074	0.200911617	0.664043045
1073	0.201280499	0.664544373
1072	0.200736218	0.663830948
1071	0.200666027	0.663904572
1070	0.201116772	0.664331741
1069	0.201013794	0.663901978
1068	0.201102085	0.663916245
1067	0.200904408	0.66451683
1066	0.201141872	0.664178391
1065	0.201157799	0.663760071
1064	0.201033421	0.663557739
1063	0.201137867	0.663512497
1062	0.200818119	0.663369064
1061	0.200688992	0.663455734

1060	0.200617485	0.662939835
1059	0.200689983	0.662801437
1058	0.200861588	0.663032761
1057	0.200403118	0.662715225
1056	0.200646915	0.662401581
1055	0.200539532	0.662106323
1054	0.200572815	0.661648331
1053	0.200410061	0.662172089
1052	0.200041504	0.661627731
1051	0.200092487	0.660852432
1050	0.199922676	0.660836945
1049	0.199753723	0.661075745
1048	0.199465008	0.660283432
1047	0.199504681	0.659918976
1046	0.199687061	0.660479126
1045	0.199232864	0.6598983
1044	0.199715157	0.659857788
1043	0.199482155	0.659124527
1042	0.199733048	0.65919838
1041	0.19936985	0.659284134
1040	0.199764595	0.659058991
1039	0.199389572	0.659481964
1038	0.199367371	0.658204041
1037	0.199904327	0.65846138
1036	0.199161472	0.658733749
1035	0.199686203	0.658135147
1034	0.199304886	0.657813263
1033	0.199527817	0.657443161
1032	0.199005318	0.657654724
1031	0.199116898	0.657400513
1030	0.199454975	0.656618271
1029	0.198940487	0.656930618
1028	0.198799915	0.655907059
1027	0.199070625	0.655871887
1026	0.198408775	0.655097275
1025	0.198682098	0.65497757
1024	0.198259926	0.655111771
1023	0.198805618	0.654132462
1022	0.19818285	0.654655151
1021	0.198330517	0.653801498
1020	0.198030472	0.653295364
1019	0.198263531	0.65296936
1018	0.197904072	0.651993713
1017	0.197746925	0.652531052
1016	0.197672672	0.651725082
1015	0.197583027	0.65174736
1014	0.197560558	0.651323776
1013	0.197385902	0.650610428
1012	0.197200756	0.65064064
1011	0.196961594	0.649802399
1010	0.196694508	0.650055618
1009	0.196539269	0.649174042
1008	0.19624939	0.648637161
1007	0.196497879	0.648792419
1006	0.196173363	0.64847786
1005	0.196630554	0.647796326
1004	0.196603012	0.647702942
1003	0.196105003	0.647424011
1002	0.196178589	0.646545563
1001	0.195975075	0.646729126
1000	0.196035614	0.646039429
999	0.195938263	0.646054459
998	0.19602766	0.645797119
997	0.195795155	0.645299835
996	0.196034145	0.645339279
995	0.195448284	0.644978943
994	0.195642929	0.644722061
993	0.195269013	0.644576111
992	0.195716953	0.644172516
991	0.194914608	0.643603821
990	0.195576172	0.643357544

989	0.195369358	0.643561401
988	0.195344791	0.643223038
987	0.195037594	0.643211975
986	0.194856186	0.642703476
985	0.195060978	0.642524262
984	0.195248165	0.642451325
983	0.195017414	0.64217186
982	0.195289326	0.641909027
981	0.194926434	0.642543259
980	0.194908924	0.64215889
979	0.19520195	0.642109985
978	0.195303612	0.64162056
977	0.19482317	0.642022858
976	0.195523052	0.641960526
975	0.194845905	0.642096787
974	0.19513298	0.642161026
973	0.195260468	0.642336807
972	0.195149212	0.64207962
971	0.195569134	0.642616425
970	0.195328865	0.642066269
969	0.195829201	0.642464218
968	0.195739536	0.643197022
967	0.195588627	0.642769394
966	0.195886154	0.642569962
965	0.195777531	0.643306885
964	0.196169148	0.643669891
963	0.196253262	0.643546906
962	0.196994839	0.644815826
961	0.196870709	0.645162811
960	0.197284279	0.645130615
959	0.197180786	0.645973663
958	0.197582207	0.64703682
957	0.197733097	0.647654495
956	0.198491764	0.648143921
955	0.198644676	0.649358597
954	0.199627247	0.650114822
953	0.199602928	0.650972061
952	0.199682674	0.652226715
951	0.200714397	0.652897797
950	0.20045002	0.653973846
949	0.20096447	0.655077057
948	0.201527023	0.656064072
947	0.201988659	0.657419128
946	0.202283726	0.657562103
945	0.20257761	0.657125626
944	0.202366791	0.658733826
943	0.203275929	0.658874741
942	0.202688446	0.659579315
941	0.203603039	0.660214996
940	0.203552113	0.660748901
939	0.204154453	0.661364822
938	0.204230099	0.661429215
937	0.204403019	0.662301331
936	0.204695053	0.663230667
935	0.20472929	0.663102951
934	0.204450188	0.664286728
933	0.205274277	0.664120941
932	0.205730534	0.664699249
931	0.205838299	0.664558563
930	0.205867214	0.66493454
929	0.205558472	0.665300674
928	0.205952473	0.665342331
927	0.205875626	0.665913315
926	0.206520863	0.66665123
925	0.206266975	0.666703186
924	0.20619751	0.66699234
923	0.206637917	0.667481384
922	0.20639307	0.666918488
921	0.206446686	0.667509842
920	0.206823368	0.667587814
919	0.207060566	0.667781372

918	0.207075424	0.668031921
917	0.207394409	0.66829834
916	0.207458839	0.667986298
915	0.207217331	0.668019486
914	0.207653484	0.668957825
913	0.207247658	0.668735657
912	0.20699997	0.668803787
911	0.207675076	0.668999863
910	0.207597332	0.668784561
909	0.207454319	0.668845673
908	0.207476578	0.668884354
907	0.207359505	0.669477768
906	0.207599983	0.669102249
905	0.207698326	0.66913971
904	0.207977657	0.669116364
903	0.207736092	0.66978569
902	0.207623959	0.669649277
901	0.207883778	0.67062027
900	0.207781048	0.669273529
899	0.207715893	0.669698868
898	0.207423115	0.669324722
897	0.207649021	0.670080948
896	0.208048439	0.669893189
895	0.207956963	0.6698423
894	0.207546539	0.670192871
893	0.208236218	0.670121689
892	0.207512264	0.670741425
891	0.207173138	0.670384979
890	0.207906189	0.670956879
889	0.208001213	0.670867233
888	0.20775507	0.670996704
887	0.207797546	0.670770493
886	0.207633667	0.670833435
885	0.207375908	0.671095581
884	0.207659893	0.671353912
883	0.207648048	0.671266403
882	0.207580261	0.671259766
881	0.207566299	0.670940857
880	0.20736908	0.671513367
879	0.207407227	0.671876221
878	0.207213097	0.671226883
877	0.207414799	0.671257858
876	0.207236843	0.671376038
875	0.207073574	0.672309494
874	0.207599392	0.671806488
873	0.207014504	0.672285233
872	0.206600304	0.671725082
871	0.207025967	0.672185211
870	0.206635666	0.672131958
869	0.206951199	0.671930771
868	0.206418285	0.672472687
867	0.20720314	0.672632294
866	0.207323322	0.673265915
865	0.206209965	0.672721176
864	0.206156654	0.673116303
863	0.20639389	0.672990265
862	0.206286125	0.672888947
861	0.206197567	0.673772202
860	0.205972748	0.673660126
859	0.206081696	0.673388443
858	0.206248112	0.673720245
857	0.205868549	0.674015732
856	0.206278	0.674200516
855	0.205682373	0.674307175
854	0.206661243	0.674389954
853	0.206446266	0.674091263
852	0.20624094	0.674512482
851	0.206420822	0.674356537
850	0.20634594	0.674862595
849	0.199481659	0.667934189
848	0.205608006	0.66930687

847	0.209320984	0.669891739
846	0.205986252	0.669384384
845	0.205046501	0.669043045
844	0.206411724	0.668615494
843	0.205765286	0.669573517
842	0.208679161	0.668695068
841	0.209084072	0.67148407
840	0.206678181	0.667689362
839	0.207738972	0.668615112
838	0.206277771	0.670520401
837	0.209238777	0.671997681
836	0.209917965	0.670046845
835	0.208657227	0.669482346
834	0.20526535	0.669588242
833	0.207433739	0.668976975
832	0.208514156	0.669658356
831	0.206077557	0.670881958
830	0.208189182	0.670560837
829	0.207668629	0.670884934
828	0.208717861	0.66973587
827	0.209298573	0.669088821
826	0.208146858	0.670397186
825	0.209945984	0.669822617
824	0.207841644	0.670567322
823	0.207108307	0.670246201
822	0.207197704	0.670018997
821	0.207439346	0.669999313
820	0.208274727	0.670813599
819	0.206742516	0.671428909
818	0.208943462	0.671739731
817	0.209528923	0.670930862
816	0.209395714	0.669782181
815	0.209885464	0.670959778
814	0.208840733	0.669609222
813	0.209466496	0.671076889
812	0.209270611	0.67080513
811	0.208440914	0.6707798
810	0.207717743	0.670018539
809	0.208301735	0.670708237
808	0.208501034	0.670566711
807	0.210072594	0.669791184
806	0.209054508	0.670367279
805	0.21053833	0.672178116
804	0.208948879	0.671333237
803	0.207989311	0.672184296
802	0.209047413	0.671180344
801	0.209324951	0.6711689
800	0.209280987	0.671418533
799	0.210035229	0.669472656
798	0.210247364	0.671139603
797	0.208700695	0.671280518
796	0.209406605	0.670794907
795	0.209474678	0.671011124
794	0.210183888	0.672017059
793	0.209151497	0.670243835
792	0.209805126	0.670658493
791	0.210160561	0.669925308
790	0.210238133	0.671666718
789	0.20879736	0.6723629
788	0.208312912	0.671266327
787	0.209581928	0.669872437
786	0.209863548	0.670638962
785	0.209508801	0.670567627
784	0.209073849	0.670310593
783	0.20997469	0.67075325
782	0.209652062	0.670653
781	0.209917488	0.671858368
780	0.210155449	0.671005249
779	0.209837761	0.670224457
778	0.21000351	0.670494156
777	0.210153885	0.670893707

776	0.209887257	0.670919037
775	0.209702587	0.669815369
774	0.210270729	0.669619598
773	0.209802361	0.670189285
772	0.209950619	0.670571594
771	0.21006424	0.670072174
770	0.210300846	0.670770187
769	0.210277615	0.670605621
768	0.209714356	0.67147789
767	0.209463749	0.670382919
766	0.210568581	0.670615997
765	0.21016861	0.6714048
764	0.209393253	0.67138916
763	0.210348511	0.670011368
762	0.209450188	0.670885544
761	0.210624809	0.671055527
760	0.209770641	0.669870758
759	0.20998806	0.671173325
758	0.20988821	0.670872421
757	0.210849609	0.670196152
756	0.210043125	0.670456162
755	0.209974804	0.670224152
754	0.210785656	0.6709832
753	0.210910606	0.67052124
752	0.210582161	0.671243134
751	0.210406532	0.671034622
750	0.210513439	0.670650864
749	0.210486946	0.670354462
748	0.210660801	0.67051506
747	0.210177498	0.669708176
746	0.210646248	0.669718475
745	0.210211258	0.670123978
744	0.210979729	0.670891647
743	0.210775414	0.670466843
742	0.210450687	0.670289688
741	0.210593185	0.670210877
740	0.210740166	0.671117249
739	0.21010601	0.669901276
738	0.210966835	0.670368652
737	0.210631542	0.670935745
736	0.210684242	0.670458832
735	0.210679894	0.671298676
734	0.21104475	0.670748444
733	0.211065807	0.670980072
732	0.21085928	0.671659088
731	0.211249695	0.670916138
730	0.211155186	0.670650635
729	0.211220684	0.670704269
728	0.211274033	0.671162491
727	0.21116745	0.670611267
726	0.211268845	0.67085846
725	0.211656723	0.670527191
724	0.211529694	0.670671616
723	0.211571789	0.670759888
722	0.211681461	0.670435486
721	0.21142334	0.671187363
720	0.21158598	0.670762177
719	0.211561375	0.671172028
718	0.211735745	0.671537094
717	0.211689816	0.671122818
716	0.211854019	0.67135376
715	0.21185257	0.67104866
714	0.211617985	0.67067131
713	0.21181879	0.671176834
712	0.211676426	0.670882645
711	0.212160778	0.671206741
710	0.212075844	0.670062103
709	0.212252216	0.670992737
708	0.2118363	0.670967255
707	0.212049313	0.670405426
706	0.211884193	0.670842438

705	0.212000675	0.670763245
704	0.212372971	0.670878143
703	0.212081738	0.670760193
702	0.212199249	0.670359345
701	0.212213135	0.671208496
700	0.212154484	0.671180954
699	0.212301292	0.670336151
698	0.212116337	0.670658188
697	0.212348194	0.670910187
696	0.212325268	0.67026062
695	0.212410145	0.670550079
694	0.212469597	0.670591736
693	0.212589836	0.670345993
692	0.212404003	0.670268173
691	0.212559967	0.670669098
690	0.212680054	0.67007988
689	0.21253542	0.670104218
688	0.212525005	0.670234833
687	0.212472954	0.670368347
686	0.212278442	0.67005249
685	0.212620201	0.670322876
684	0.212414227	0.670267563
683	0.212432003	0.670540466
682	0.212512035	0.669943543
681	0.212539024	0.670153275
680	0.212539444	0.670015183
679	0.212651138	0.670145645
678	0.212708798	0.669974442
677	0.212610283	0.669940414
676	0.212878399	0.670187988
675	0.212826157	0.669922028
674	0.212780476	0.669782944
673	0.212697105	0.66984436
672	0.212681294	0.669570236
671	0.212782383	0.669522858
670	0.212791748	0.669774857
669	0.212919178	0.669523926
668	0.212947369	0.669747009
667	0.212882481	0.66969307
666	0.212725716	0.669481735
665	0.212852516	0.669252167
664	0.212723637	0.669149704
663	0.212744427	0.669234467
662	0.212874279	0.669539871
661	0.212849522	0.669157105
660	0.212910423	0.668837662
659	0.212853203	0.669200821
658	0.212839222	0.669340515
657	0.213010006	0.668971634
656	0.212960911	0.669062195
655	0.212964878	0.668904495
654	0.213015652	0.669210968
653	0.212980919	0.669269943
652	0.212937679	0.66908699
651	0.213044376	0.66917366
650	0.213159981	0.668947678
649	0.212976112	0.669237213
648	0.213062477	0.668768845
647	0.213258438	0.668963699
646	0.213238392	0.668741913
645	0.213175163	0.668694382
644	0.213243694	0.668625336
643	0.213452797	0.66837822
642	0.213471565	0.668756332
641	0.213504982	0.668683929
640	0.213375588	0.668561325
639	0.213527165	0.668377609
638	0.213675671	0.668157578
637	0.213658466	0.66867775
636	0.213713684	0.668341065
635	0.213462715	0.668223724

634	0.213639336	0.668430786
633	0.213795853	0.668327637
632	0.21370348	0.668396683
631	0.213772259	0.668369064
630	0.213860493	0.668233185
629	0.213893642	0.668197861
628	0.213841763	0.668542557
627	0.213916168	0.668185425
626	0.213984928	0.667792358
625	0.214358196	0.668233719
624	0.214178524	0.668110809
623	0.214094734	0.66809639
622	0.214336815	0.667979889
621	0.214318581	0.668074265
620	0.2143717	0.667688141
619	0.214226341	0.667651596
618	0.214406052	0.66746048
617	0.21427042	0.66775856
616	0.214434643	0.66800148
615	0.214206276	0.667326584
614	0.21420414	0.667799606
613	0.214438629	0.667433548
612	0.214238815	0.667584076
611	0.214346123	0.667546234
610	0.214535809	0.667358551
609	0.214399376	0.66739975
608	0.21432991	0.667272186
607	0.214338322	0.667133331
606	0.214511776	0.667188568
605	0.21437458	0.667038879
604	0.214346981	0.66691246
603	0.214367962	0.666939163
602	0.214452477	0.666884308
601	0.214504356	0.666584168
600	0.214581299	0.6667482
599	0.214327564	0.666698608
598	0.214610634	0.666632919
597	0.21463089	0.66654419
596	0.214744244	0.666176453
595	0.214888001	0.666513825
594	0.214892387	0.666258621
593	0.2152108	0.666588364
592	0.215089359	0.666380615
591	0.215366669	0.666081009
590	0.215219269	0.665986939
589	0.215148621	0.666041412
588	0.21546217	0.66608139
587	0.215103607	0.666103668
586	0.215265369	0.66580925
585	0.215412178	0.665870438
584	0.215373688	0.666086044
583	0.215281124	0.665439682
582	0.215439262	0.665551987
581	0.215183849	0.665550156
580	0.215419846	0.665447693
579	0.215389843	0.665446854
578	0.215730457	0.665393601
577	0.215914326	0.665151825
576	0.216252594	0.665148163
575	0.215865326	0.665216293
574	0.215888119	0.66492775
573	0.215771866	0.664735413
572	0.215924473	0.665002441
571	0.215801678	0.664791412
570	0.216057587	0.664587174
569	0.216105366	0.664235992
568	0.215910339	0.66482193
567	0.215877514	0.664434128
566	0.216055145	0.66449997
565	0.216023636	0.664411316
564	0.216070347	0.664153824

563	0.216058636	0.663724747
562	0.215980701	0.663747101
561	0.216011848	0.66381897
560	0.21596426	0.663786316
559	0.215885468	0.663611984
558	0.215798168	0.6631073
557	0.215975666	0.66338913
556	0.215667057	0.662850342
555	0.215933991	0.66259613
554	0.215674095	0.663275909
553	0.21567297	0.662516708
552	0.215483093	0.662425919
551	0.215494652	0.662505722
550	0.215695572	0.66235527
549	0.215524674	0.662105255
548	0.215649986	0.661952133
547	0.215445156	0.661684113
546	0.215405331	0.661339035
545	0.215435505	0.661527939
544	0.215630932	0.660867691
543	0.215222664	0.66077507
542	0.215135193	0.660638351
541	0.215189018	0.660584183
540	0.214995956	0.660748749
539	0.21510416	0.660352402
538	0.214935627	0.66022583
537	0.214729843	0.659620056
536	0.214814224	0.659580612
535	0.214712563	0.659503861
534	0.214869862	0.659370575
533	0.214587536	0.659171677
532	0.214431934	0.659145966
531	0.214502716	0.658523483
530	0.214209042	0.658262787
529	0.214385872	0.658275528
528	0.214359112	0.657584992
527	0.21416605	0.657733765
526	0.214215698	0.657344971
525	0.214118366	0.657825089
524	0.213796711	0.656949997
523	0.213703232	0.656585083
522	0.213488064	0.656676178
521	0.213485031	0.656611023
520	0.213396244	0.65633728
519	0.213529339	0.655720749
518	0.213413677	0.655966034
517	0.213180447	0.655569305
516	0.213116264	0.654949646
515	0.212905045	0.655484314
514	0.212717133	0.655060196
513	0.212650719	0.654816895
512	0.212423763	0.654163055
511	0.212378235	0.653673782
510	0.212878189	0.653274689
509	0.212135773	0.653362274
508	0.212204704	0.652844162
507	0.211967354	0.652671433
506	0.211817246	0.652239838
505	0.211837101	0.652512054
504	0.211428013	0.651508713
503	0.21120739	0.651443405
502	0.211123791	0.650812073
501	0.210973015	0.650552445
500	0.210876331	0.650094299
499	0.210615521	0.649960632
498	0.210562592	0.649466782
497	0.210095329	0.649236527
496	0.210047035	0.648614578
495	0.20992054	0.648580856
494	0.209531536	0.647828064
493	0.209432049	0.647294464

492	0.209330387	0.647286377
491	0.209128552	0.646620865
490	0.208773289	0.646210098
489	0.208715057	0.64611145
488	0.208272362	0.644940872
487	0.208252468	0.644733505
486	0.20784956	0.644155197
485	0.207682495	0.643600998
484	0.207288723	0.643195953
483	0.206994038	0.64246872
482	0.206735973	0.642369843
481	0.206488915	0.64178978
480	0.206040478	0.640782318
479	0.205891647	0.640893326
478	0.205526581	0.640048523
477	0.205204086	0.63938736
476	0.204741497	0.638687363
475	0.204510593	0.638191986
474	0.204225979	0.63728859
473	0.203886471	0.636854401
472	0.203519993	0.636057129
471	0.203065739	0.635524826
470	0.202671566	0.634450264
469	0.202339935	0.633868218
468	0.201537342	0.63329464
467	0.201514053	0.632397766
466	0.200996151	0.631762428
465	0.200632343	0.630655937
464	0.200093575	0.630126953
463	0.199757328	0.629501534
462	0.19919817	0.628128815
461	0.198620625	0.627504158
460	0.198133507	0.626679649
459	0.197877426	0.625837135
458	0.197340431	0.624615746
457	0.196652584	0.623924904
456	0.196087856	0.622716789
455	0.195742302	0.621868591
454	0.195146236	0.620921364
453	0.194586315	0.619836807
452	0.193965206	0.618670883
451	0.193319912	0.617927094
450	0.192776775	0.617151032
449	0.192440682	0.615652313
448	0.191755905	0.614357109
447	0.191115227	0.613212166
446	0.190512543	0.612601776
445	0.189859715	0.610869751
444	0.189470139	0.609754677
443	0.18850462	0.60859211
442	0.187923279	0.607836838
441	0.187359333	0.60576416
440	0.186589413	0.604864006
439	0.185896912	0.603641167
438	0.185054207	0.602042198
437	0.184476509	0.601067352
436	0.18397789	0.599507408
435	0.183299465	0.597908859
434	0.182411022	0.596798134
433	0.181657867	0.594849091
432	0.180930786	0.59394043
431	0.179993668	0.592085419
430	0.179396019	0.590507164
429	0.178359871	0.588706741
428	0.177462959	0.586831818
427	0.176479263	0.585130997
426	0.175532723	0.582977829
425	0.174101181	0.580643425
424	0.172934437	0.579057999
423	0.171549759	0.576160545
422	0.170023861	0.573539963

421	0.168832912	0.570405846
420	0.16746254	0.567348557
419	0.165815373	0.564023438
418	0.164038658	0.560861282
417	0.162106266	0.557052002
416	0.160476246	0.553982506
415	0.159204197	0.551417885
414	0.158590031	0.550240326
413	0.158461914	0.548815613
412	0.158536673	0.548622971
411	0.158704367	0.547451668
410	0.157927971	0.545894737
409	0.157175674	0.54419445
408	0.156613169	0.542533951
407	0.155804501	0.54025322
406	0.154531803	0.538392601
405	0.153359022	0.53546936
404	0.152484865	0.533458939
403	0.151067343	0.531019859
402	0.150026083	0.528335114
401	0.149121027	0.525772705
400	0.147248831	0.522824478
399	0.146312609	0.520478745
398	0.144824696	0.517367706
397	0.143935471	0.514602356
396	0.142454605	0.512380524
395	0.140952702	0.509439888
394	0.139814491	0.505616264
393	0.138371048	0.501870232
392	0.136509743	0.498319626
391	0.134828987	0.494473801
390	0.133335962	0.489942017
389	0.131782217	0.486272926
388	0.130472546	0.483168907
387	0.130025177	0.481042328
386	0.129259224	0.479109154
385	0.128963232	0.476588669
384	0.128418236	0.474408073
383	0.127135353	0.470794334
382	0.126204147	0.468148842
381	0.124733334	0.464822426
380	0.12374548	0.461076927
379	0.122219429	0.458330689
378	0.121364498	0.45474926
377	0.120057631	0.450890312
376	0.118770275	0.447116585
375	0.117547483	0.443147469
374	0.115999069	0.439419403
373	0.115054836	0.435211449
372	0.113807087	0.43187954
371	0.112544823	0.427857742
370	0.111321678	0.424364967
369	0.1103508	0.420584831
368	0.109180708	0.416467743
367	0.108452768	0.412710609
366	0.107053833	0.409347992
365	0.106933346	0.405866242
364	0.106009598	0.402896957
363	0.105211144	0.399849739
362	0.104661446	0.39623867
361	0.103603334	0.392293549
360	0.102686691	0.388015289
359	0.101129599	0.383577843
358	0.100320168	0.379452477
357	0.099676952	0.374862785
356	0.098416414	0.370686455
355	0.097178507	0.36557354
354	0.096084232	0.360250931
353	0.095265446	0.354749336
352	0.093919306	0.349265633
351	0.092281456	0.344528008

350	0.091751041	0.338529472
349	0.088165312	0.323861198
348	0.091396828	0.317200432
347	0.088740072	0.310997582
346	0.087215805	0.303994122
345	0.088616123	0.29725132
344	0.085093718	0.2910676
343	0.086833267	0.284845409
342	0.084125767	0.277358742
341	0.0812076	0.269868259
340	0.079825878	0.263717384
339	0.079255896	0.256614304
338	0.081493702	0.251039772
337	0.078532162	0.243998375
336	0.078395925	0.237454529
335	0.076285191	0.231883221
334	0.077951975	0.225418148
333	0.076489501	0.219543037
332	0.073721371	0.214031601
331	0.073804607	0.206249275
330	0.07172946	0.200243263
329	0.072899475	0.194252167
328	0.072390714	0.187758217
327	0.068558507	0.181133709
326	0.071098537	0.175081615
325	0.067845812	0.168640957
324	0.068960652	0.16236702
323	0.068055749	0.155816259
322	0.067287445	0.149586391
321	0.066068425	0.142738876
320	0.064978213	0.136885862
319	0.066358047	0.130039129
318	0.064272313	0.123502207
317	0.06284718	0.117916603
316	0.062084689	0.112112656
315	0.063471565	0.106264153
314	0.061104407	0.100039454
313	0.05922863	0.094042015
312	0.06060863	0.087976494
311	0.060016336	0.08266614
310	0.059340067	0.077086425
309	0.056723213	0.070924187
308	0.057082934	0.065842571
307	0.056982183	0.060201473
306	0.056162219	0.055288553
305	0.05604094	0.050085821
304	0.056671066	0.045503001
303	0.05671566	0.040752506
302	0.056498113	0.036582322
301	0.05532382	0.032166314
300	0.054073248	0.028557103
299	0.053903894	0.025238981
298	0.052749558	0.021905184
297	0.052718472	0.018878993
296	0.052495675	0.016093125
295	0.051790218	0.013894305
294	0.052355099	0.011665131
293	0.05156189	0.00992153
292	0.050802579	0.00842301
291	0.050690875	0.007028485
290	0.050926566	0.005885406
289	0.051763644	0.005015383
288	0.051238151	0.004162937
287	0.049901419	0.003626278
286	0.051149259	0.003134084
285	0.049110851	0.002735465
284	0.050108538	0.002335918
283	0.050134683	0.002005673
282	0.049469523	0.00185042
281	0.050056295	0.001691161
280	0.050780749	0.00167614

279	0.050141897	0.001603802
278	0.049377079	0.001499044
277	0.050622973	0.001405542
276	0.049883614	0.001498721
275	0.050171876	0.001363746
274	0.050372567	0.001500517
273	0.050036035	0.001291562
272	0.050841579	0.001505789
271	0.051101623	0.001492438
270	0.050967088	0.001461076
269	0.05066525	0.001506442
268	0.051183023	0.001581504
267	0.052653251	0.001645923
266	0.052160835	0.001668578
265	0.052045646	0.001781906
264	0.051865258	0.001836079
263	0.052248006	0.001884671
262	0.051835189	0.00201371
261	0.05195106	0.002065681
260	0.051548023	0.002124035
259	0.0529285	0.002319485
258	0.052102971	0.002476545
257	0.053375478	0.002539616
256	0.053320351	0.002674763
255	0.053376718	0.00280791
254	0.054506407	0.002904432
253	0.053598199	0.002997473
252	0.053261585	0.003343258
251	0.053577466	0.003457771
250	0.054828501	0.003842553
249	0.055676622	0.00401432
248	0.056141953	0.004364449
247	0.056530895	0.004613899
246	0.057159295	0.004825211
245	0.057543883	0.004998183
244	0.058106465	0.005142503
243	0.058504672	0.005278601
242	0.058401518	0.00549525
241	0.059090428	0.005884761
240	0.0594384	0.006103919
239	0.060438657	0.006416344
238	0.061764469	0.006640267
237	0.061926341	0.006771944
236	0.062443995	0.007098128
235	0.063288188	0.00715408
234	0.063636632	0.00719914
233	0.064104772	0.007573076
232	0.064199524	0.007852378
231	0.065357738	0.007942105
230	0.065947905	0.008340392
229	0.065893383	0.00844741
228	0.067273798	0.008551495
227	0.067628155	0.008796725
226	0.066478124	0.00891439
225	0.067336745	0.009407033
224	0.066067867	0.009716721
223	0.068792157	0.010117747
222	0.068886919	0.010246886
221	0.06927897	0.010482239
220	0.069046698	0.010839431
219	0.069879198	0.011178373
218	0.069464183	0.011007891
217	0.071164699	0.011398801
216	0.07107439	0.011845404
215	0.069854679	0.011929212
214	0.072655201	0.012417655
213	0.074280119	0.012458223
212	0.074066768	0.013075105
211	0.073894596	0.013202311
210	0.074536481	0.013186562
209	0.077600985	0.014076141

208	0.07517767	0.014674156
207	0.078339853	0.01473551
206	0.085334721	0.015387437
205	0.091959829	0.015939412
204	0.096646614	0.016488208
203	0.09076498	0.017244812
202	0.096257372	0.018708057
201	0.095578108	0.019135664
200	0.090631981	0.020591502